



Effect of sulphur on the structure of silicate melts under oxidizing conditions

Yann Morizet, Michael Paris, Ida Di Carlo, Bruno Scaillet

► To cite this version:

Yann Morizet, Michael Paris, Ida Di Carlo, Bruno Scaillet. Effect of sulphur on the structure of silicate melts under oxidizing conditions. *Chemical Geology*, 2013, 358, pp.131-147. 10.1016/j.chemgeo.2013.09.004 . insu-00873919

HAL Id: insu-00873919

<https://hal-insu.archives-ouvertes.fr/insu-00873919>

Submitted on 18 Oct 2013

HAL is a multi-disciplinary open access archive for the deposit and dissemination of scientific research documents, whether they are published or not. The documents may come from teaching and research institutions in France or abroad, or from public or private research centers.

L'archive ouverte pluridisciplinaire **HAL**, est destinée au dépôt et à la diffusion de documents scientifiques de niveau recherche, publiés ou non, émanant des établissements d'enseignement et de recherche français ou étrangers, des laboratoires publics ou privés.

EFFECT OF SULPHUR ON THE STRUCTURE OF SILICATE MELTS UNDER
OXIDISING CONDITIONS.

Y. MORIZET¹, M. PARIS², I. DI CARLO³, B. SCAILLET³

¹ Université de Nantes, Nantes Atlantique Universités, Laboratoire de Planétologie et
Géodynamique de Nantes (LPGN)

UMR CNRS 6112

2 rue de la Houssinière, 44322 NANTES (France)

² Institut des Matériaux Jean Rouxel (IMN), Université de Nantes

UMR CNRS 6502

2 rue de la Houssinière, BP32229, 44322 NANTES Cedex 3 (France)

³ CNRS/INSU-Université d'Orléans – BRGM

UMR 7327

Institut des Sciences de la Terre d'Orléans

1a rue de la Férollerie, 45071, Orléans, France

Corresponding author: Dr Yann Morizet

Permanent address:

Laboratoire de Planétologie et Géodynamique de Nantes (LPGN), Université de Nantes

CNRS/INSU – UMR CNRS 6112

2 rue de la Houssinière, BP 92208.

44322 Nantes Cedex 3 (FRANCE).

Email: yann.morizet@univ-nantes.fr

Tel: +33 (0) 2 5112 5491

Fax: +33 (0) 2 5112 5268

Abstract:

In magmatic systems, sulphur is an important volatile element after C, H and O. Under oxidising conditions, S dissolves in aluminosilicate melt as sulfates groups (SO_4^{2-}). The way SO_4^{2-} groups dissolve in the melt is currently poorly understood. We present experimental results of the effect of SO_4^{2-} dissolution on the aluminosilicate melt structure.

Glasses of haplogranitic (HPG) and anorthite-diopside eutectic (An-Di) compositions were synthesised at 300 MPa and 1250°C and under oxidising conditions ($\Delta\text{FMQ}+1.7$ to $+3.0$). Starting compositions were equilibrated under fluid-saturated conditions with a mixture of S (0 to 5 wt.%) and H_2O (5 wt.%). The S and H_2O contents of the recovered glasses were determined with EPMA and FTIR, respectively. Solid State NMR was used to investigate the glass structure. Micro-Raman analyses were performed to identify S species present in glass and coexisting fluid phases.

The S content determined in glasses changes from 0 to 979 ppm and 0 to 7519 ppm for HPG and An-Di, respectively. S is present in the glasses as $\text{M}^{n+}\text{SO}_4^{2-}$ groups (M^{n+} is possibly Ca^{2+} in An-Di and Na^+ in HPG).

^{29}Si NMR analyses show important changes in the An-Di glass structure upon S dissolution. High S content in An-Di glasses induces a strong polymerisation of the glass which we explain by the presence of Non-Bridging Oxygen (NBO) promoting the dissolution of S as SO_4^{2-} groups. On the contrary, the dissolution of S within HPG melt does not produce visible changes in the silicate melt structure due to the low concentration in NBO in this melt composition.

The observed structural changes suggest that An-Di melt physical properties might be affected by S dissolution. S might produce large changes in melt viscosity, but opposite, as compared to H₂O for slightly depolymerised aluminosilicate melts.

Number of words: 289.

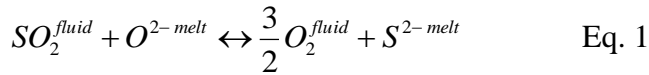
Keywords: sulphur dissolution mechanism, silicate glass speciation, Solid-State NMR, silicate glass viscosity.

1. Introduction:

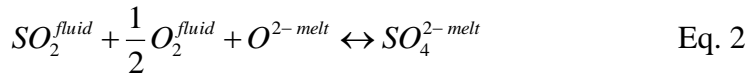
Sulphur (S) is an important volatile element in magmatic systems. The S output from volcanic emissions to the atmosphere has contributed greatly to the change in the chemistry of the Earth or other planets atmospheres (e.g., Gaillard and Scaillet, 2009; Gaillard et al., 2011). Although this element is stored in small quantities in the Earth interior (e.g. McDonough and Sun, 1995; Dreibus and Palme, 1996; Jugo et al., 2005a; Gaillard et al., 2013), it can take a large part of the fluid phase in many volcanic eruptions (e.g., Scaillet et al., 2003). Hence, the eruptive degassing of a large reservoir for S can have a dramatic impact on the climate (Oppenheimer et al., 2011).

The behaviour of S in silicate melts is not fully understood. One major experimental difficulty lies in the different oxidation state that S can take as a function of fO_2 conditions. S can be present as S^{2-} and S^{6+} for the most important species (e.g. Fincham and Richardson, 1954; Carroll and Rutherford, 1988; Paris et al., 2001; O'Neill and Mavrogenes, 2002; Fleet, 2005; Jugo et al., 2005a, 2010; Moretti and Ottonello, 2005; Wilke et al., 2008; Klimm and Botcharnikov, 2010; Baker and Moretti, 2011; Métrich and Mandeville, 2010). The S content measured in silicate glass is dependent on fO_2 conditions experienced. Early studies conducted at 1 atm with gas mixture furnace (Fincham and Richardson, 1954; Katsura and Nagashima, 1974) showed that a minimum in S solubility in glasses synthesized at $\log fO_2 = -5$ or -6 and between 1200 and 1300°C. This minimum in S content is generally ascribed to a minimum in sulphur species fugacities (Carroll and Webster, 1994) in the gas phase.

Under oxidizing conditions, S is dissolved in silicate glass as sulphate (SO_4^{2-}) groups whereas it dissolves as sulphide (S^{2-}) groups under more reducing conditions (e.g. Carroll and Rutherford, 1988; Métrich and Clocchiatti, 1996; Jugo et al., 2005a, b). The dissolution of S is defined by two chemical reactions involving the interaction with a fluid phase (Fincham and Richardson, 1954):



and



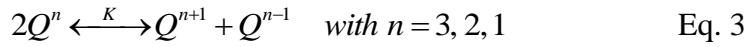
The Eq. 1 applies to the dissolution of S in silicate melts under reducing conditions and Eq. 2 applies to the dissolution of S under oxidizing conditions.

The composition of the melt greatly influences the solubility of S with a central role for FeO (Haughton et al., 1974; Carroll and Webster, 1994; O'Neill and Mavrogenes, 2002; Beermann et al., 2011; Baker and Moretti, 2011), SiO_2 (Moretti and Ottonello, 2005), and possibly H_2O in FeO-poor melts (Clemente et al., 2004, Prouteau and Scaillet, 2013).

A silicate glass in the broad sense (a melt containing SiO_2) is a combination of several individual structural units, called Q-species (e.g. Grimmer et al., 1984; Brandiss and Stebbins, 1988; Merzbacher et al., 1990; Stebbins, 1995; Mysen and Richet, 2005) where Q represents a SiO_4 tetrahedron and is considered as a network forming unit. In complex silicate melts where other oxides than SiO_2 are present, Al_2O_3 is also considered as a network forming cation (AlO_4 tetrahedra) whereas other cations (for example, Ca, Mg,

Na and K) are either network modifiers or charge balancing cations (e.g. Neuville and Mysen, 1996; Lee and Stebbins, 2000).

The notation Q^n is often employed where n represents the number of bridging oxygen (BO) per tetrahedron. The abundance of each Q^n species is controlled by the following general equation (e.g. Maekawa et al., 1991; Mysen and Frantz, 1993; Frantz and Mysen, 1995; Malfait et al., 2007):



where K is the equilibrium constant of the reaction. Thus, the structure and physical properties (in particular viscosity) of a silicate glass are related through the distribution of these different Q^n units (e.g. Mysen, 1998; Neuville, 2006; Malfait et al., 2007). It is currently assumed that the Q^n distribution (Eq. 3) in glasses will represent the equilibrium frozen-in at the glass transition temperature, T_g (e.g. Brandiss and Stebbins, 1988; Farnan and Stebbins, 1994; Maekawa and Yokokawa, 1997). The presence of volatile species induces a change in this equilibrium reaction. In particular, H_2O plays a major role in silicate melt by breaking the bonds in between tetrahedra changing a BO in NBO (non-bridging oxygen) therefore inducing a depolymerization of the silicate melt (e.g. Farnan et al., 1987; Kummerlen et al., 1992; Zotov and Keppler, 1998; Zeng et al., 1999; Xue and Kanzaki, 2004; 2008; Xue, 2009).

Although Eq. 2 is generally accepted for the S dissolution mechanisms in silicate melts under oxidising conditions, the role of Eqs. 1-2 on Eq. 3 is currently unknown. In other words, both the effect of S on the physical properties of silicate and the way S atoms

influence the melt structure, hence Eq. 3, are unclear. Recent work conducted at high pressure in the $\text{Na}_2\text{O-SiO}_2$ system by Tsujimura et al. (2004) suggests that S produces a change in the network structure of silicate glass. They concluded that the dissolution of S involves the polymerization of the melt resulting from a change in the melt composition as Na is exsolved into the fluid phase. This possible mechanism needs to be explored further by conducting experiments on more complex silicate glass compositions of geological interest.

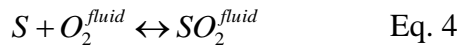
We present experimental results aimed at investigating the possible effects of S on the silicate glass structure with implications on silicate melt physical properties. We have chosen two different starting compositions reflecting two different melt structures: one fully polymerized (only BOs, $\text{NBO} = 0$) and one slightly depolymerized (both BOs and NBOs are present). The experiments were conducted at 300 MPa and 1250°C under oxidizing conditions. The spectroscopic results are discussed in term of polymerization / depolymerization of the glass upon S dissolution and the impact of this finding is discussed in term of the qualitative effect of S as compared to the effect of H_2O onto the silicate melt physical properties.

2. Experimental method:

The synthetic haplogranitic (HPG) and anorthite-diopside eutectic (An-Di) compositions in the $\text{Na}_2\text{O-K}_2\text{O-Al}_2\text{O}_3\text{-SiO}_2$ and $\text{CaO-MgO-Al}_2\text{O}_3\text{-SiO}_2$ systems were prepared from a mixture of oxides (SiO_2 , Al_2O_3 and MgO) and carbonates (Na_2CO_3 , K_2CO_3 and CaCO_3). The absence of iron is imposed by the analytical needs for investigating the melt speciation with NMR which cannot be used on Fe-bearing materials. The theoretical

compositions are reported in Table 1 along with the electron probe micro-analyses (EPMA) for major elements of all the samples. The starting compositions were prepared by mixing all oxides and carbonates together and by melting the powders twice at 1400°C for a few hours.

Elemental sulphur (up to 1 wt.% S for HPG, up to 5 wt.% for An-Di) was added to the starting powders prior the experiments by thorough grinding in an agate mortar ensuring homogeneous distribution down to a 100 micron scale (see Table 2). During the experiments, the S combines with available O atoms to oxidize as sulphates (SO_4^{2-}). For instance, S can oxidize by combining with available O present in the fluid phase following Eq. 4:



The H_2O was added as liquid water together with the solid starting material in the platinum capsules. As shown in Table 1, the initial water content (Initial H_2O) ranges from 1.5 to 4.9 wt.% for HPG samples and from 3.9 to 4.9 wt.% for An-Di samples. We synthesized several S-free samples and with different H_2O content (see Table 1, for example HPG-5-0 and AD-5-0) so the individual effect of H_2O and S on the glass structure can be compared. For these S-free samples, the synthesised glasses are undersaturated with respect to H_2O solubility. At 300 MPa and 1250°C, we estimated the H_2O solubility at 6.2 and 6.5 wt.% for AD and HPG glass composition according to the H_2O solubility model VolatileCalc (Newman and Lowenstern, 2002) for both HPG and AD compositions.

The sample nomenclature is organized as follows: the letters indicate the composition, the first number gives the initial H_2O loaded and the second number gives the initial S

content loaded into the experiments. For example, AD-5-0 corresponds to the sample synthesized with 5 wt.% H₂O and 0 ppm S added to the charge.

Because compositional changes with S dissolution in An-Di melt composition were observed (see section 4), we also synthesized three volatile-free glasses with different MgO content. Those glasses are reported in Table 1 and denoted as AD (9.2 wt.% MgO), AD+2 wt.% MgO (10.6 wt.% MgO) and AD-2 wt.% MgO (7.0 wt.% MgO). The three glasses were synthesized at 1400°C and 1 bar. In doing so, we tried to mimic the change in the wt.% MgO observed in S-bearing glasses synthesized at high pressure (see Table 1).

Experiments were conducted in an Internally Heated Pressure Vessel (IHPV) at 1250°C and 300 MPa and for run duration of 3 hours. Recent work (e.g., Liu et al., 2007; Beermann et al., 2011) suggest that under those experimental conditions, such run durations allow equilibrium conditions to be reached. We have calculated the diffusion length (Zhang, 2010) using the diffusivity equation of Freda et al. (2005) for hydrous basalt. After 3h, the diffusion is less than a mm in length suggesting our run duration is long enough to reach equilibrium distribution of S at the capsule scale, though in the richest S-bearing experiment (AD-5-5) heterogeneity was noted (see below). We stress, however, that any heterogeneous distribution of S across the capsule will be averaged out by the fact that NMR technique is a bulk method probing the structure of the entire sample.

The procedure to achieve the experimental conditions is described in detail elsewhere (e.g., Scaillet et al., 1992). The IHPV is loaded at room temperature with a known partial pressure of Argon to roughly half the desired total pressure (P^{tot}) value (150 MPa). The

temperature is then brought to the final value and the P^{tot} increases up to requested experimental pressure (300 MPa). P and T are constantly monitored during the experiment using an electronic gauge for P and an S-type thermocouple connected to a Eurotherm controller for T. The T gradient along the capsule is measured with an additional S-type thermocouple and does not exceed 5°C. P, T measurements are accurate to within ± 20 bars and $\pm 5^\circ\text{C}$, respectively.

The experiments were carried out under oxidizing conditions as imposed by the intrinsic $f\text{O}_2$ conditions of the vessel. The $f\text{O}_2$ relative to FMQ buffer is basically estimated at $\Delta\text{FMQ} = +3$ (Pichavant et al., 2009; Lesne et al., 2011). However, because the experiments were conducted undersaturated with respect to H_2O content, the $f\text{O}_2$ experienced by the samples during the experiments is below this highly oxidised conditions (see Table 1). The determination of the $f\text{O}_2$ conditions experienced by each sample will be discussed further in section 4.1.

The sample is quenched to near ambient temperature ($<50^\circ\text{C}$) by dropping the capsules into the cold part of the IHPV, with a quench rate on the order of $150^\circ\text{C}/\text{s}$ for that kind of apparatus (Di Carlo et al., 2006; Iacono-Marziano et al., 2008). In all cases, opening of the capsules produced a hiss (with a smell of S) indicating that a fluid phase was present in the capsule during the experiment.

Several chips from the recovered glasses were selected for micro-Raman, micro-FTIR and EPMA analyses. The remaining of the glass sample was then crushed for MAS NMR analyses. Optical examination of the glass reveals the presence of randomly distributed round shaped fluid inclusions, as observed by Morizet et al. (2009), giving a cloudy aspect to the glass. Within those inclusions we did not identify the presence of crystalline

sulphates. Such bubbles (made of S-O-H species) will be transparent to ^{29}Si - and ^{27}Al -NMR analyses. The loaded S is in excess as compared to S content dissolved in the glass, and such an excess S likely resides in the coexisting fluid phase; the grey aspect of the outer glass surface possibly results from quench precipitation of S at the capsule-melt interface, a feature not occurring within bubbles. The most S-rich samples, had a slightly coloured brownish glass.

3. Analytical techniques:

3.1 S content and major element concentrations obtained by EPMA:

The sulphur and major elements concentrations were measured using EPMA. Measurements were done on a Cameca SX 50. For S analysis we used four PET wavelength-dispersive crystals spectrometers, using the following analytical conditions: accelerating voltage 15 kV, sample current 50 nA, and a peak counting time on each spectrometer of 60 s, with a total counting time of 240 s. For major elements we used instead 15kV and 10 nA, with 10 s peak counting time for all elements. Na and K were first analyzed and a PAP correction procedure was applied. Na possible migration under the beam was corrected by using secondary hydrous glass standards of known Na_2O and H_2O contents (Clemente et al., 2004). Analyses were conducted in defocused mode (10 μm beam diameter) in order to avoid any elemental loss. SEM analyses did not reveal any heterogeneity in the sample major element concentrations.

The average major elements concentrations obtained on more than 20 points analyses for the recovered glasses are reported in Table 1. The standard deviation for each oxide is below 1.0 wt.% for most An-Di glasses (AD-4-0 shows a larger variation >1.0 wt.% in

SiO₂). The most important variation is observed for HPG glasses where standard deviation for SiO₂ is above 1 wt.%. The S content determined in the glasses was calibrated using glass standards. The three used synthetic hydrous dacitic standard glasses have S content at 750, 1400 and 1900 ppm. The error on the S analyses was obtained from at least 20 EPMA points for each sample (see Table 2). The S solubility was measured on several glass chips to check for heterogeneities within each sample as shown in Table 2.

3.2 *Micro-Raman for S speciation in glass:*

Confocal micro-Raman was used to characterize the S speciation within the glasses. The Raman system is a Jobin-Yvon Labram spectrometer (focal distance = 300 mm) equipped with a 2400 gratings/mm CCD detector. The light source is an Ar laser Innova 300-5W from Coherent© operating at 514.5 nm. The typical output laser power was set to 50 mW. The analyses were performed in confocal mode (hole = 500 µm, slit = 200 µm) with an Olympus (x50) objective. The spectral frequency position was measured with the emission lines of Ne- and Hg-lamps. The accuracy is within $\pm 1 \text{ cm}^{-1}$.

The acquisition time for the different glass samples is relatively short and is usually within 30-60 s to obtain a reasonably good signal to noise ratio (S/N). All spectra are normalized to the same acquisition time for relevant quantification.

The spectra were investigated between 400 and 1200 cm^{-1} showing the silicate framework vibrational signature as well as the S species dissolved in the glass. We also acquired spectra in the 2500 cm^{-1} to check for the presence of HS groups (Klimm et al., 2012a; see Supplementary material).

3.3 *Micro-FTIR for H₂O content:*

Doubly polished plates were prepared from selected glass sections for micro-FTIR analyses in order to quantify the H₂O^{tot} content of the glass. Mid- and Near-IR spectra (between 1000 and 6000 cm⁻¹) were obtained for 100x100 µm spot size using a Continuum[®] microscope attached to a Nicolet[®] 5700 Fourier transform infrared spectrometer. A KBr beamsplitter and MCT-B detector were used to collect 128 scans (for sample and background) at a resolution of 4 cm⁻¹. The atmospheric contribution (in particular atmospheric water) was reduced by enclosing the sample in a box purged with dry air during at least 20 minutes before analysis. Prior to sample acquisition, an instrumental background was taken to subtract the atmospheric contribution. Several spectra (>3) were taken on different selected locations (optically bubble-free) in the glass plate and results show that H₂O is evenly distributed across the sample. A volatile-free FTIR spectrum was taken on the An-Di and HPG dry glasses and was subtracted from each spectrum obtained for volatile-bearing samples. Thickness measurements were done with a Mitutoyo[®] digitometer with an accuracy of ±1 µm on the doubly polished sample plate (<300 µm). All spectra were normalized to 100 µm for quantitative analysis.

The H₂O^{tot} quantification was done using the Beer-Lambert law (Eq. 5, e.g. Stolper, 1982; Behrens et al., 1996):

$$C_i = \frac{MM_i \times Abs}{d \times \rho \times \epsilon_i} \quad \text{Eq. 5}$$

which relates the concentration of the identified species (C_i) to the FTIR peak absorbance (Abs), the molecular mass of the i species (MM_i), the density of the glass (ρ), the thickness of the analyzed chip (d) and the molar extinction coefficient (ϵ_i).

The FTIR spectra show two clear peaks at 4500 and 5200 cm^{-1} corresponding to OH groups and $\text{H}_2\text{O}^{\text{mol}}$, respectively. The total water content ($\text{H}_2\text{O}^{\text{tot}}$) is the sum of the two species concentrations determined via the Beer-Lambert law. The area of each peak (OH and $\text{H}_2\text{O}^{\text{mol}}$) was determined from hand-fitted baseline.

The HPG and An-Di glass densities were calculated with the model of Lange and Carmichael (1987): 1) 2219 g.L^{-1} for HPG, 2) 2645 g.L^{-1} for An-Di.

We quantified each species with integrated molar extinction coefficients (ϵ_i). There are several values for integrated molar extinction coefficient for OH and $\text{H}_2\text{O}^{\text{mol}}$ species.

Those values are dependent on the glass composition (Mandeville et al., 2002). For HPG, we used the integrated values derived by Withers and Behrens (1999): 1) 310 $\text{L.mol}^{-1}.\text{cm}^{-2}$ for OH species, 2) 257 $\text{L.mol}^{-1}.\text{cm}^{-2}$ for $\text{H}_2\text{O}^{\text{mol}}$. Unfortunately, there is no available integrated extinction coefficient for H_2O species dissolved in An-Di glass. We tried to use the value determined by Stolper (1982): 1) 200 $\text{L.mol}^{-1}.\text{cm}^{-2}$ for OH species, 2) 300 $\text{L.mol}^{-1}.\text{cm}^{-2}$ for $\text{H}_2\text{O}^{\text{mol}}$; however, those values appear to be unsuitable for this type of investigated composition and strongly underestimate the total water content. For instance, if we consider AD-5-0 and AD-4-0, both samples were synthesised in S-free conditions. The initial H_2O content loaded in the capsule prior to the experiments is 4.85 and 3.93 wt.%, respectively. Using the extinction coefficient from Stolper (1982), the H_2O content measured in the recovered glasses is 3.24 and 2.30 wt.%, respectively. Those derived values are inconsistent with the calculated water saturation level (>6 wt.%) at 300 MPa

and 1250°C derived from VolatileCalc model (Newman and Lowenstern, 2002). At 300 MPa and 1250°C, the measured H₂O content should be close to the initial loaded H₂O. Consequently, to obtain a reliable estimate of the H₂O content, we had to apply a correction factor of x1.6 (i.e. $4.85/3.24 = 1.496$ for AD-5-0 and $3.93/2.30 = 1.709$) to the initially derived taking into account the under estimation of the H₂O content using Stolper (1982) extinction coefficient for AD samples. Unfortunately, no independent method was available to quantify the individual extinction coefficient for each water species. Owing to the fact that we used the same approach for the whole set of sample, such a quantification is broadly consistent in relative terms.

All results for H₂O^{tot}, OH and H₂O^{mol} are reported in Table 1. The H₂O^{tot} values are the average values calculated from the FTIR spectra collected on a given sample (see Supplementary material for all measured FTIR values for H₂O^{tot}) and is the sum of the species concentrations (OH+H₂O^{mol}). The error bars are the standard deviation determined from the H₂O^{tot} obtained on the FTIR spectra. The error (± 0.2 wt.% H₂O on average) is typical when estimating the H₂O concentrations from FTIR spectroscopic method (e.g., Morizet et al., 2010). We observe that the H₂O^{tot} determined for HPG samples is higher than the H₂O loaded into the Pt capsules. This difference can be due to the presence of moisture into the starting material. At 300 MPa 1250°C, the H₂O solubility level is higher than the loaded H₂O. In other words, the H₂O content in our HPG experiments is below the water saturation for those experimental conditions (Schmidt et al., 1999; 2001). It suggests that the H₂O^{tot} can exceed the total H₂O loaded into the experiment if adsorbed water is present at the beginning. The presence of

adsorbed water is likely due to the fine grained nature of our starting materials (which were not stored in an oven).

3.4 *MAS-NMR for melt and water speciation:*

The ^{27}Al and ^{29}Si Solid State MAS NMR experiments of the partially crushed samples were acquired on a 500 MHz Bruker Avance III ($B_0 = 11.7\text{ T}$). A 4 mm Triple channel CP/MAS probe was employed and the samples loaded in a ZrO_2 rotor with Teflon end-cap. Rotors were spun at 10 or 14 kHz. The measurements were made at the Larmor frequency of the different nuclei: 130.326 and 99.352 MHz for ^{27}Al , ^{29}Si , respectively. Spectra are referenced against TMS (Tetramethylsilane) for ^{29}Si and $\text{Al}(\text{NO}_3)_3$ in aqueous solution for ^{27}Al . The NMR analytical conditions which we used to analyse our glass samples are reported in the Supplementary material.

The ^{29}Si MAS NMR spectra were acquired with single $\pi/4$ excitation of 2 μs . The spectra were acquired with proton decoupling (except for AD-5-0 and AD-5-1) so as to avoid any broadening of the ^{29}Si spectrum due to the coupling with ^1H (Laws et al., 2002). The recycle delay for the ^{29}Si acquisition was set to 15 s. The ^{29}Si -species can have long spin lattice relaxation time in silicate glasses (several minutes, Maekawa et al., 1991). We tested several recycle time D1 values (15 to 150 s) to check for the consistency in the response of the Si-species. No noticeable difference in terms of line shape and chemical shift signatures was observed (only the peak absolute intensity will change) in the resulting spectra suggesting that all ^{29}Si species have similar spin-lattice relaxation.

Several spectra were acquired under $\{^1\text{H}\}$ - ^{29}Si CPMAS conditions for HPG samples (see Supplementary material). The proximity between ^1H and ^{29}Si atoms can be investigated

using this method. The ^{29}Si acquisition is conducted with 2 and 5 s recycle delays. The contact time (c.t.) for the transfer of magnetization is 1 or 2 ms.

The ^{27}Al spectra were acquired for all the glass samples with single $\pi/12$ with a radiofrequency field of 16 kHz with proton decoupling. We used D1 of 1 and 2 s which is standard for ^{27}Al spin relaxation in silicate melts (Lee and Stebbins, 2000) or crystals (Begaudeau et al., 2012).

In all the spectrum acquisitions (^{29}Si and ^{27}Al), we collected a large number of scans to obtain a good S/N ratio. Between 256 and 2,048 scans have been co-added (see Supplementary material).

4. Results:

4.1 S, H₂O contents and $f\text{O}_2$ estimate in the An-Di and HPG melts:

The Figure 1 shows the S content determined from EPMA analyses. The results are reported for An-Di (Figure 1A) and for HPG (Figure 1B) (see Table 2 for numerical values). The open symbols in Figure 1 correspond to the S content measured on different glass chips for each composition whereas the black symbols are the S average content determined. The error bars for the open symbol correspond to the standard deviation of at least 20 analyses on each chip. We considered an average of the different S analytical sessions as representative of the total S content of the glasses synthesized. The error on the filled symbol is the standard deviation calculated from the different chips S content analysis. For HPG, the error on S content is relatively small (below ± 100 ppm) suggesting that HPG glass samples are homogeneous in S content. For An-Di, the variability in S content is higher. Except for AD-5-5, which had an heterogeneous S

distribution, on average the error on S solubility is about 10% of the total content, being similar to that of previous similar studies (e.g. Jugo et al., 2005a). The generally higher dispersion observed for the S-richest samples clearly relates to the overall low diffusivity of S in silicate melts (e.g., Watson, 1994).

For AD-5-5, two different glass chips were analysed resulting in S contents at 9921 ± 402 and 5117 ± 107 ppm S. This large dispersion in S content is due to heterogeneity within the sample, showing that bulk equilibrium for this particular sample was not achieved. However, as already stated, the NMR measurement is a bulk analysis which will average out the possible heterogeneities. We will consider to a first approximation that the average between the EPMA analyses sessions for AD-5-5 is representative of the bulk S content in this sample.

The S content (see Table 2) ranges up to 7519 ppm and up to 979 ppm for An-Di and HPG glasses, respectively. The HPG glasses exhibit a lower S content than An-Di for a given bulk S content. For a bulk S content of ~ 10000 ppm, the S content in AD-5-1 is more than three times higher than the S content in HPG-5-1 (see Table 2). The observed S content in HPG glasses is similar to that of previous studies. Under oxidizing conditions for hydrous rhyolite, Clemente et al. (2004) reported a maximum of 1200 ppm for S solubility at 1000°C and 200 MPa. For An-Di, there are no prior experiments but comparison can be made with studies on hydrous basaltic systems performed under similar P and T conditions. Reported S contents range from 0.3 wt.% (Moune et al., 2009: Hekla basalt) up to 1.1 wt.% (Beerman et al., 2011: Etna basalt), hence bracketing the S content of An-Di glasses obtained here. Although the SiO_2 content is supposed to induce substantial changes in the dissolved S content (see Moretti and Ottonello, 2005), we

suspect that other oxides (in particular alkaline-earth cations, Ca and Mg) are playing a major role in the S content. For both compositions studied An-Di and HPG, the S content increases with increasing total S loaded. This observation is consistent with previous investigations (e.g., Clemente et al., 2004; Moune et al., 2009).

The $\text{H}_2\text{O}^{\text{tot}}$ content determined from FTIR measurements is shown next to each point ranging from 2.23 ± 0.14 to 5.39 ± 0.30 wt.% for HPG glasses; and from 2.70 ± 0.09 to 5.18 ± 0.48 wt.% for An-Di. For An-Di samples, the $\text{H}_2\text{O}^{\text{tot}}$ is lower than the initial H_2O loaded for S-bearing synthesised glass samples.. For these samples, the water activity ($a(\text{H}_2\text{O})$) during the experiments for An-Di samples with mixed H_2O -S fluid phase is different from unity (i.e. $a(\text{H}_2\text{O}) < 1$) due to water molar fraction different from unity in the fluid phase (e.g., Dixon et al., 1995), therefore resulting in a H_2O content lower than H_2O solubility in the quenched glass.

The water speciation as determined from FTIR measurements is reported in Table 1. For HPG glass samples, the water speciation is similar between the HPG samples except for HPG-1.5-0 which was loaded with lower initial H_2O content. The OH content changes from 2.06 to 2.47 wt.%. The $\text{H}_2\text{O}^{\text{mol}}$ content ranges from 2.20 to 2.92 wt.%.

For An-Di glass samples, the water speciation is also similar between the samples except for AD-5-0 which exhibits a higher water content relative to other AD samples. The OH content ranges from 1.62 to 3.31 wt.%. The $\text{H}_2\text{O}^{\text{mol}}$ content ranges from 0.71 to 1.87 wt.%. We suggest that the water speciation in glasses is similar in between the samples for each set of glass HPG and An-Di. Besides, the calculation of the NBO/T (Non Bridging Oxygen per Tetrahedron) for each sample includes the effect of OH dissolution (see section 4.2). It should be emphasised that the calculated NBO/T represents a helpful

basis for comparison and interpretation; however, it does not represent the true degree of polymerisation. For instance, Stebbins and Xu (1997) reported the presence of NBO in anorthite glass nominally fully polymerised ($\text{NBO}/T = 0$).

Due to the water-undersaturated nature of experimental syntheses, the initial estimate of the $f\text{O}_2$ at FMQ+3 cannot be applied. This derived value from Lesne et al. (2011) and Pichavant et al. (2009) can only be applied if the experimental conditions are vapour-saturated which is not applicable in the present study (see section 3.3). We have recalculated the $f\text{O}_2$ conditions using the intrinsic $f\text{H}_2$ of the IHPV (~ 1 bar) during the experiments and the $f\text{H}_2\text{O}$ in the fluid phase derived from VolatileCalc (Newman and Lowenstern, 2002) and determined from the $\text{H}_2\text{O}^{\text{tot}}$ (see Table 1). The $f\text{O}_2$ values are reported in Table 1. As we can see, the $f\text{O}_2$ values differ from the suggested FMQ+3. For HPG samples, the $f\text{O}_2$ ranges between +1.7 to +2.9 relative to FMQ buffer; for AD samples, the $f\text{O}_2$ is ranging between +1.8 and +2.8 relative to FMQ buffer. We do not expect a significant change in S speciation in this interval of $f\text{O}_2$ variation in agreement with previous studies on Fe-free compositions (Klimm et al., 2012b).

4.2 *S and glass composition: Major elements concentration and NBO/T*

The glass compositions are shown in Table 1. The first line for each composition represents the theoretical composition. The major element concentrations for HPG glasses are consistent (except for Na) within error to the theoretical composition. The maximum variability is observed for SiO_2 with an error of up to ± 1.85 wt.% for HPG-1.5-0 glass. Concentrations in Na_2O (and to a lesser extent K_2O) are slightly lower than the

nominal value (~ 3.7 vs ~ 4.6 wt.%, respectively, see Table 1) which possibly reflect transport of this element into the coexisting fluid phase.

The variation in major elements concentrations is much more important for An-Di glass composition, possibly as a result of element transport into the coexisting fluid; however, within the whole set of An-Di samples and within the major elements variation observed, it is still possible to decipher the effect of S dissolution on the glass structure. We show in Figure 2 the variability in the An-Di glass composition for the synthesized samples expressed as the molar $\text{MgO} / \text{MgO} + \text{CaO}$ ratio (Figure 2A) and the molar $\text{Al}_2\text{O}_3 / \text{Al}_2\text{O}_3 + \text{SiO}_2$, as these two ratios are classical descriptors of the structure of silicate glasses.

In Figure 2A, we observe that the $\text{MgO} / (\text{MgO} + \text{CaO})$ ratio ranges between 0.35 and 0.45 with a standard deviation which is less than 0.040. In detail, four experiments have values at 0.35 and therefore similar in term of glass structure. In Figure 2B, we show the molar $\text{Al}_2\text{O}_3 / (\text{Al}_2\text{O}_3 + \text{SiO}_2)$ ratio variability observed for An-Di glasses. The determined values are close to 0.150 with a small variation which does not exceed 0.004 and therefore can be considered negligible.

We calculated the NBO/T for the An-Di glasses and show the change in S content as a function of this parameter in Figure 3. The NBO/T was calculated using the method of Mysen (1988, 1990). We considered in the NBO/T calculation the depolymerizing effect of water onto silicate melt structure. The dissolved water has a structural role similar to that of network modifying cations, that is, it induces the formation of NBO by breaking the bridges between tetrahedra. Therefore, we have considered that all the OH present in the glass, as measured by FTIR (see Table 1), acts as a network modifying cation. For

this calculation the $\text{H}_2\text{O}^{\text{mol}}$ is not taken into account. A similar treatment has been recently applied by Iacono-Marziano et al. (2012).

For An-Di glass samples, the calculated NBO/T values range from 1.044 (AD-5-5) to 1.248 (AD-5-0) and for a theoretical value of 0.921 (see Table 1). The observed change in the degree of polymerization ($1.04 < \text{NBO/T} < 1.25$) results from the change in H_2O concentration as well as in major element concentrations amongst glass samples. In Figure 3 we observe that several An-Di samples with different S content have similar NBO/T with a change of less than 0.05; hence such samples will be considered in priority for investigating the change in the melt structure that could arise from varying S contents. The NBO/T value has been also calculated for HPG samples. The HPG composition is initially fully polymerized ($\text{NBO/T} = 0$). However with OH present (see Table 1), the NBO/T (calculated with the effect of water taken into account) is different from 0 and ranges between 0.072 and 0.156.

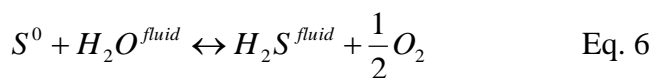
4.3 *S speciation from Micro-Raman spectroscopy in glass.*

We investigated our synthesized glass samples via Micro-Raman spectroscopy to check for the presence of vibrational signatures of sulphates and additional S compounds. The results are shown in Figure 4 (A for An-Di, B for HPG) for two samples with S (AD-5-5 and HPG-5-1) and without S (AD-5-0 and HPG-5-0). We present also in Supplementary material several spectra for fluid inclusions and glasses in the region for HS vibrational signature at 2500 cm^{-1} .

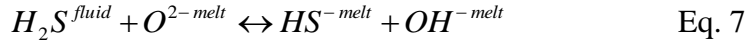
In Figure 4A, besides the strong signature for the aluminosilicate framework in the range $400\text{-}1100 \text{ cm}^{-1}$ (Frantz and Mysen, 1995; Mysen, 1999; Neuville et al., 2006), we observe

in AD-5-5 an intense broad peak at 997 cm^{-1} which we attribute to ν_1 S-O stretching vibration in sulphate molecules (e.g. Lenoir et al., 2009; Klimm and Botcharnikov, 2010; Wilke et al., 2011, Klimm et al., 2012a, b) consistent with our oxidizing conditions. This peak is totally absent in the spectrum of S-free AD-5-0 sample. Despite the oxidizing conditions ($\Delta\text{FMQ} > +1.8$) imposed during our experiments, we observe a small fraction of sulphides (HS^-) present in the An-Di glass samples and showing a Raman signature at $\sim 2575\text{ cm}^{-1}$ (Klimm et al., 2012a, b). We estimated the HS^- content dissolved in the glass with the method described by Klimm et al. (2012b) which correlates the Raman signature of the 990 cm^{-1} for sulphate groups and the 2575 cm^{-1} for sulphide groups to the $\text{S}^{6+}/\text{S}^{\text{Total}}$. The results are reported in the Supplementary material. For AD-5-5 showing the most intense HS^- signature, the concentration of reduced S species is less than 3% (i.e. 97% are SO_4^{2-}). For the other samples, the intensity of the HS^- signature is too low to get any reasonable estimate of the sulphide concentration. The presence of less than 3% HS^- in the dissolved S is consistent with previous results obtained under oxidizing conditions (e.g. Jugo et al., 2005b).

We have analysed fluid inclusions in a few samples (see Supplementary material). The Raman spectra of the fluid inclusions revealed the presence of H_2S fluid species but did not show any evidence for the presence of crystalline CaSO_4 suggesting that anhydrite saturation was not reached. The presence of H_2S in the fluid and HS^- in the glass implies that reaction described by Eq. 4 is not the only one occurring and a reaction involving reduced S-species is also occurring, such as:



In Eq. 6, the loaded elemental S combines with the hydrogen of the water molecules to form H₂S in the fluid. The H₂S is then dissolved in the melt as HS⁻ groups (Carroll and Webster, 1994; Clemente et al., 2004; Baker and Moretti, 2011; Prouteau and Scaillet, 2013) following Eq. 7:



We have compared our spectra for An-Di to the Raman spectrum obtained for crystalline compounds. A spectrum for gypsum (CaSO₄·2H₂O) taken from the RUFF[®] database is reported in Figure 4A. The gypsum Raman spectrum has a very strong vibrational signature around 1000 cm⁻¹ which comforts our assignment for the peak at 997 cm⁻¹ and the presence of sulphate groups in AD-5-5. The broad aspect of the peak at 997 cm⁻¹ as compared to the peak for crystalline gypsum suggests that the SO₄²⁻ groups are dissolved within the melt and not present as crystalline sulphates.

Additional vibrational signatures are seen in AD-5-5 spectrum. We identified two peaks at 213 and 464 cm⁻¹. Those peaks are weak in intensity but sharp in shape. The sharpness of these peaks suggests that it might correspond to crystalline compounds. We propose an assignment to elemental S in agreement with previous studies (e.g. White, 2009; Tsujimura et al., 2004 and reference therein). The presence of elemental S coating the outer surface of glass is in agreement with the excess S present during our experiments, arising possibly from quench crystallization in the fluid during cooling in a way similar to that occurring during hydrothermal processes (Giggenbach, 1980, 1987).

We also observed an intense peak located at 532 cm⁻¹ in AD-5-5 but absent in AD-5-0.

The assignment of this peak is uncertain. Previous studies (Chivers et al., 1978; Ahmed et

al., 1997; Tsujimura et al., 2004) suggested the existence of a similar peak at 535 cm^{-1} and assigned it to radical S_3^- anions in silicate melts.

The Raman spectra for HPG-5-0 and HPG-5-1 in Figure 4B are almost identical. In contrast to An-Di, there is no appearance of additional Raman signature upon S dissolution. The solubility level is different between the two compositions: $\sim 1000\text{ ppm S}$ for HPG-5-1, $\sim 7000\text{ ppm S}$ for AD-5-5. Hence, the peak for S-O stretching mode in sulphate is hidden by the aluminosilicate framework vibrational signature at 1000 cm^{-1} . However, it is possible to see a small sharp peak around 1144 cm^{-1} which could correspond to exsolved crystalline sulphate. This position is very close to the one observed by Tsujimura et al. (2004) for crystalline Na_2SO_4 at 1150 cm^{-1} . Two additional peaks at 219 and 472 cm^{-1} weak in intensity are attributed to elemental S, as for AD samples (see above).

4.4 *Glass speciation from NMR measurements:*

4.4.1 ^{29}Si NMR signature:

The glass structure was investigated via ^{29}Si NMR using single pulse and $\{^1\text{H}\}$ - ^{29}Si CPMAS sequences. The spectra obtained for each sample are reported in Figure 5. The spectra for S- H_2O -bearing and S-free H_2O -bearing are shown for An-Di in Figure 5A and for HPG in Figure 5B. The spectra for volatile-free An-Di with various MgO contents are reported in Figure 5C. The spectra are characterized by a single peak showing a slight asymmetry. For An-Di samples in Figure 5A, the asymmetry is visible on the low frequency side (more negative values) whereas for HPG samples in Figure 5B, the asymmetry is visible on the high frequency side (less negative values) but less

pronounced than for An-Di samples. The existence of an asymmetric peak for the ^{29}Si NMR signature suggests that several structural Q-species environments are present within the melt.

We reported also in Figure 5B $\{^1\text{H}\}$ - ^{29}Si CPMAS spectra for several samples with and without S. There is a clear shift toward less negative value for the peak maximum at ~ -97.8 ppm.

We reported next to each spectrum the maximum peak position as determined from the spectra (values are also given in Table 3). From Figure 5A and B, we notice a significant difference in the maximum peak position between An-Di and HPG. For An-Di samples, we determined a maximum peak position close to -86 ppm whereas for HPG samples, the maximum is seen around -104 ppm (-97.8 ppm for $\{^1\text{H}\}$ - ^{29}Si CPMAS spectra). This difference can be explained by the difference in composition. The HPG composition is more silica-rich and more polymerized ($\text{SiO}_2 = 78.6$ wt.%; $\text{NBO/T} \sim 0$) than An-Di ($\text{SiO}_2 = 50.2$ wt.%; $\text{NBO/T} \sim 1.0$). A correspondence is found between the ^{29}Si NMR ppm shift and the degree of polymerization (e.g. Lippmaa et al., 1979; Smith et al., 1983; Emerson et al., 1989; Maekawa et al., 1991; Stebbins, 1995). For fully polymerized melt like HPG, the silicate framework is mostly composed of Q^4 units ($\text{NBO} = 0$ and $\text{BO} = 4$) and will show low frequency position (< -100 ppm) in the ^{29}Si NMR peak as established in previous studies (Schramm et al., 1984; Brandiss and Stebbins, 1988; Maekawa et al., 1991; Kummerlen et al., 1992; Schmidt et al., 2001).

The spectra for each composition are also reported in Figures 5A and B as a function of increasing S content. In Figure 5A, we observe a shift in the peak maximum as a function of S content. In S-free samples the peak position is less negative whereas in S-bearing the

peak maximum position is more negative. When comparing AD-4-0 (1.072,0) and AD-5-5 (1.044,7519) (two samples having a similar NBO/T), we observe a shift between the peak maximum of -1.6 ppm with increasing S content.

For S-free samples, when comparing AD-4-0 (1.072,0) and AD-5-0 (1.248,0), we observe a shift of +1.2 ppm between the peak maximum. This shift is correlated with the increase in the NBO/T (1.072 to 1.248). This increase in the NBO/T is attributed to the change in OH content (see Table 1; 3.31 for AD-5-0 and 2.39 for AD-4-0) as the depolymerizing effect of OH onto the NBO/T is taken into account in our calculation.

The positive shift in the ^{29}Si NMR peak position is consistent with previous investigations of the effect of water on the glass structure (Farnan et al., 1987; Zeng et al., 2000; Robert et al., 2001; Cody et al., 2005). The ^{29}Si NMR peak position will be shifted toward less negative values accounting for the change from Q^n to Q^{n-1} in the depolymerization process. The S dissolution seems to produce the opposite effect. The change from -84.1 to -85.7 ppm between S-free and AD-5-5 with 7519 ppm S is in favor of a polymerizing effect of S. We do not observe changes in the single pulse ^{29}Si NMR spectra for HPG samples (Figure 5B). The peak maximum does not seem to change as a function of S suggesting that at the measured S level (~1000 ppm) there is no observable changes in the Si environments.

For example, for similar NBO/T (~0.12), the S-free HPG-4-0 sample has a peak maximum at -103.6 ppm and S-bearing (979 ppm S) HPG-5-1 sample has a peak maximum at -104.0 ppm. The -0.4 ppm change cannot be attributed unambiguously to a change in S content.

The purpose of Figure 5C is to assess the possible effect of the slight compositional changes that have been observed for An-Di samples (see Figure 2 and 3). In Figure 5C, we present the ^{29}Si NMR spectra for volatile free An-Di glasses synthesized at 1 bar and 1400°C and with various MgO contents (7.04, 9.23 and 10.63 wt.% MgO). We observe a shift in the peak maximum position as a function of MgO content. Between 7.04 and 9.23 wt.% MgO, a slight displacement toward higher frequency is observed -84.5 to -83.7 ppm. Similarly, between 9.23 and 10.63 wt.% MgO, a shift toward higher frequency is seen, from -83.7 to -82.9 ppm. On average, the addition of 1 wt.% MgO induces a decrease of less than 1 ppm in the ^{29}Si NMR peak maximum consistent with a depolymerisation of the glass with increasing network modifying cations. This variation is well below the observed variation in ppm shift upon S dissolution. For example, between AD-4-0 and AD-5-5, the MgO variation (9.09 and 8.91 wt.% MgO, respectively) cannot explain the shift in the peak maximum from -84.1 to -85.7 ppm. Hence we conclude that the change in S content from 0 to 7519 ppm is the major factor influencing the ^{29}Si NMR maximum peak.

4.4.2 ^{27}Al NMR signature:

We have acquired ^{27}Al MAS NMR spectra for several samples of the different compositions An-Di and HPG. The spectra are shown in Figure 6: A, for An-Di; and B, for HPG.

The spectra vary between the compositions. We can see that An-Di samples in Figure 6A have ^{27}Al NMR spectra showing multiple Al environments. The line shape of the spectra shows a prominent peak at +55 ppm for the peak maximum consistent with Al atoms are

in 4-coordination (^{IV}Al). There is an apparent shoulder located at roughly +30 ppm in favor for additional 5-coordinated Al (^{V}Al); a peak around 0 ppm also suggests the presence of 6-coordinated Al atoms (^{VI}Al). Those peak positions are consistent with previous identifications (see Stebbins, 1995; Toplis et al., 2000). The presence of highly coordinated aluminium is in agreement with previous findings for similar compositions Stebbins et al. (2000). The abundances of ^{V}Al and ^{VI}Al are probably low in our samples: less than 10% as suggested by studies on similar glasses either anhydrous (Toplis et al., 2000; Stebbins et al., 2008) or hydrous (Xue and Kanzaki, 2008).

The three coordination states are observed for all the An-Di samples regardless of the total amount of S and H_2O . We show in Figure 6A the difference between the AD-5-1 and AD-5-0. This difference does not result in a flat signal but show several features suggesting that subtle changes in the spectra line shapes are occurring. The difference in between the two spectra shows a depression at $\sim +65$ and 0 ppm. The observed changes are very low and not necessarily due to S dissolution. Between AD-5-1 and AD-5-0 the change in H_2O content is large (2.81 and 5.18 wt.%, respectively) and such a variation might induce change in ^{27}Al NMR spectral signature as suggested by previous studies (Kohn et al., 1989; Schmidt et al., 2001; Padro et al., 2003; Malfait et al., 2012).

The ^{27}Al spectra for HPG samples in Figure 6B show the presence of only ^{IV}Al environment. When comparing HPG-4-0 (0,4.26) and HPG-5-1 (979,4.28), no change in the spectrum line shape is observed. We also reported in Figure 6B the difference in between the HPG-5-1 and HPG-5-0 spectra. The difference signal is almost flat suggesting a weak change in the Al environment upon S and H_2O dissolution.

5. Discussion:

5.1 *S speciation in silicate glasses under oxidizing conditions*

The micro-Raman spectra in Figure 4 show that S is mainly dissolved as sulphate groups in both compositions in agreement with the oxidizing conditions ($\Delta FMQ > +1$) and consistent with Eq. 2. Yet, it is yet not clear if there is a particular affinity of S for either Ca or Mg. Both elements are often suggested to present the same structural behaviour in silicate glasses acting as network modifiers or charge balancing cations (Taylor and Brown, 1979). However, slight differences can be observed between cations having different ionic radius and field strength (Shannon and Prewitt, 1969). A recent compilation by Wilke et al. (2011) suggests that SO_4^{2-} groups are preferentially associated with network modifying cations with a Raman shift depending on the surrounding cation field strength.

The additional vibrational signature observed corresponds to a small amount of sulphide (3% HS^-) dissolved in the glass samples with the highest S content (AD-5-5). The presence of small amounts of HS^- in An-Di glass is also confirmed by the fact that we did not observe any dramatic changes in the water speciation. Recent work by Stelling et al. (2011) showed that the water speciation was correlated with the presence of reduced HS groups with the appearance of an additional H_2O signature at 3400 cm^{-1} in the FTIR spectra. Such vibrational signature was not observed in our Raman spectra in agreement with the estimated low concentration in HS^- groups in our samples. Furthermore, we have conducted additional FTIR measurement on unpolished S-bearing glass chip in the H_2O^{tot} region at 3500 cm^{-1} and did not find evidence for similar vibrational signature at 3400 cm^{-1} . In addition the coexistence of both sulphate and sulphide species might be due to a

lower water activity in the melt (Stelling et al., 2011). However, the concentration of HS^- in the S-rich An-Di glass samples is subordinate to the SO_4^{2-} concentration and the expected change in water activity is probably low considering the fact that most of the An-Di glasses exhibit similar water speciation (see Table 1).

Under highly oxidizing conditions ($\Delta\text{FMQ}+3$), S is dissolved in glass solely as sulphate groups; the presence of sulphide implies that the $f\text{O}_2$ experienced during the experiments is lower than the $f\text{O}_2$ necessary to observe only sulphate groups. We have calculated the diminution in $f\text{O}_2$ in presence of 3% of reduced HS^- species which corresponds to the highest HS^- content observed in our samples (i.e. AD-5-5). We used the empirical equation derived by Zajacz et al. (2012) (see also Jugo et al., 2010). According to Zajacz et al. (2012), a change in $\text{S}^{6+}/\text{S}^{\text{tot}}$ from 1 to 0.97, corresponds to a decrease in $f\text{O}_2$ by less than 0.5 log unit. Therefore, any decrease in $f\text{O}_2$ is assumed to be negligible. It is also consistent with the reported $f\text{O}_2$ obtained from the dissolved H_2O content and reported in Table 1: $f\text{O}_2 > \text{FMQ}+1.7$ for HPG samples, $f\text{O}_2 > \text{FMQ}+1.8$ for AD samples. The departure from fully oxidised conditions ($\text{FMQ}+3$) does not induce a dramatic change in S speciation in agreement with recent work on Fe-free glass compositions (Klimm et al., 2012b).

An additional vibrational signature at 532 cm^{-1} is identified from the Raman spectra in Figure 4. Its assignment remains uncertain. One hypothesis is the presence of S_3^- anionic radicals. The presence of such S unit is surprising owing to our highly oxidized experimental conditions. The S_3^- species have been previously identified in silicate melts (Ahmed et al., 1997) or in hydrothermal solutions (Pokrovski et al., 2011). We are however sceptic about this possible assignment and the presence of anionic radicals S_3^- ,

because of the lack of NMR evidence as discussed below. S_3^- anionic radicals dissolve in silicate melts by replacing a non-bridging oxygen atom (with only one negative charge) of the SiO_4 tetrahedra (Ahmed et al., 1997; Winther et al., 1998). The net result of this dissolution mechanism is to form $Si-S_3^-$ bond which can be clearly identified by NMR. Pradel et al. (1995) investigated the change in δ_{iso} chemical shift of ^{29}Si in chalcogenide glasses. The observed ^{29}Si δ_{iso} for glasses containing four $Si-S^-$ bonds is located in the NMR spectrum between -20 and +10 ppm. Due to the high intensity of the 532 cm^{-1} in the Raman spectrum, it might be possible that, if present, $Si-S^-$ bonds will induce a strong signature in ^{29}Si NMR spectrum. We did not identify such a signature in the ^{29}Si NMR spectra in any An-Di samples, which therefore argue against the existence of anionic S_3^- assignment of the 532 cm^{-1} Raman peak. Moreover, such anionic radicals are observed in alkali-rich (>10 mol.%) glass compositions (Ahmed et al., 1997). The investigated compositions (An-Di is alkali-free) in our study do not match the requirements for anionic radicals to exist.

5.2 *Change of structural of Si and Al upon SO_4^{2-} dissolution based on NMR simulation*

Using appropriate fitting of the ^{29}Si NMR spectra, it is possible to investigate quantitatively the change in silicate glass structural units Q^n species.

For HPG glass composition, with NBO/T close to 0, Q^4 species should be the most abundant structural unit. Q-species with a lower degree of polymerization should be less abundant. As shown in Figure 5B, $\{^1H\}$ - ^{29}Si CPMAS NMR analyses reveal that the ^{29}Si NMR spectrum for HPG is a combination of several different Q-species.

The fitting performed on the ^{29}Si NMR spectra of all the samples and for both An-Di and HPG glass compositions are shown in Figure 7 (A, An-Di; B, HPG). For clarity, the obtained fits on ^{29}Si NMR spectra for An-Di with various MgO content are not shown. The results of the fits for all the samples are reported in Table 3. We should emphasize the fact that such spectral simulations are not unique and present just one, among other, solutions.

The fitting were performed in several steps on the entire dataset simultaneously for a given composition. Firstly, we placed under the spectra envelope two or three Gaussian peaks. Initially, the peak positions and width were fixed and the amplitude for each Gaussian was optimized. Secondly, the peak position was left free to evolve for a fixed width. Thirdly, the width and position were left free to evolve. The two last steps were repeated several times so as to obtain the lowest value for the chi-square ($\chi^2 = 0.012$ and 0.5 for HPG and An-Di, respectively). The fitting were conducted with Origin© fitting software package following a Levenberg-Marquardt algorithm.

In Figure 7A, we observe that each An-Di spectrum is well reproduced by the fitting with three Gaussians. The three peaks have respective δ_{iso} position at -79.9, -86.8 and -95.3 ppm. The derived width (FWHM) is 4.6, 4.9 and 6.4 ppm, respectively. The error on each δ_{iso} and FWHM value is less than ± 0.1 as given by the software (see Table 3).

A possible assignment is also proposed for each Gaussian peak in An-Di glasses. The peak at -79.9 ppm is attributed to Q^2 species. For glasses synthesized in the CaO-SiO_2 system (close to our An-Di composition), similar δ_{iso} for Q^2 species have been reported at ~ -80 ppm by previous work (Zhang et al., 1997; Schneider et al., 2003). For alkali silicate melts, the signature for Q^2 species is identified at $\delta_{\text{iso}} \sim -80$ ppm (e.g. Grimmer et al.,

1984; Maekawa et al., 1991; Malfait et al., 2007). The second peak at -84.7 ppm is assigned to Q^3 species in accordance with previous NMR investigations (Zhang et al., 1997; Schneider et al., 2003). The peak at -95.3 ppm has a chemical shift similar to Q^4 species with Al as next nearest neighbour (e.g. Merzbacher et al., 1990; Sykes et al., 1997). The number of Al as the second nearest neighbour is uncertain; however, considering the Si/Al ratio for An-Di glass (~5.5), the probability for finding more than 1 Al atom in the surrounding of the Si Q^4 unit is relatively low (less than 15%).

We observe that the S dissolution influences dramatically the amplitude of the Q^4 peak (Figure 7A). Hence, we cannot propose a single assignment to this peak. In S-free samples, the peak at -95.3 ppm can be assigned to Q^4 species but in S-bearing we suggest that a more complex species is formed from the polymerization of Q^3 or Q^2 units. For instance, this species will be denoted as Q^{4*} .

As a function of S content and despite the variable $H_2O - S$ initial contents, there is a clear increase in the amplitude of the peak at -95.3 ppm and for a similar NBO/T (comparison between AD-4-0 and AD-5-5 at NBO/T1.072 and 1.044). This increase occurs along with a decrease in the amplitude of the peak at -79.9 ppm suggesting that the dissolution of S induces a net polymerization of the melt. At first sight, the peak at -86.8 ppm assigned to Q^3 units does not seem to change in amplitude as a function of S. Hence, the dissolution of S appears to be favored by the presence of the lowest polymerized units. It also suggests that the solubility of S in silicate melts might be enhanced by the increase in NBO/T which has been suggested by previous studies (e.g. Holzheid and Grove, 2002; Backnaes and Deubener, 2011 and references therein).

In Figure 7B, the simulation results for HPG glass samples are shown. In contrast to An-Di spectra, the simulation was performed with only two Gaussian peaks in agreement with single pulse ^{29}Si and $\{^1\text{H}\}\text{-}^{29}\text{Si}$ CPMAS NMR data shown in Figure 5B. The assignment of the individual Gaussian is based on the work of Schmidt et al. (2000). For fully polymerized melts in the quartz – albite system, Schmidt et al. (2000) simulated ^{29}Si NMR spectra considering the proximity of Al atoms. The peak located at -105.3 ppm is attributed to $\text{Q}^4(0\text{Al})$ (Q^4 unit surrounded by four SiO_4 tetrahedra). The presence of Al surrounding the SiO_4 tetrahedra changes the ^{29}Si NMR chemical shift by several ppm toward higher frequency. The peak at -98.9 ppm could be assigned to $\text{Q}^4(1\text{Al})$ (Q^4 unit surrounded by three SiO_4 tetrahedra and one AlO_4 tetrahedra) or $\text{Q}^3(0\text{Al})$ following the work of Schmidt et al. (2000). This assignment takes also into account the probable distribution of Al atoms surrounding SiO_4 tetrahedra. The Al molar fraction is too low (i.e. $\text{Si}/\text{Al} \sim 10.7$) to favor the presence of two Al atoms surrounding an SiO_4 tetrahedron. We also calculated the probability to find 2 Al atoms surrounding an SiO_4 tetrahedron. This probability is below 5% and the most probable units present in HPG are Q^4 and Q^3 surrounded by either 0 or 1 Al atoms. The possibility for Q^3 species to be present in HPG glass composition is consistent with the fact that the calculated NBO/T is different from 0 (values at ~ 0.1 , see Table 1). Hence, our HPG glass samples are not fully polymerized due to the dissolution of OH groups.

The effect of S on the abundances of each species is subtle. The effect of S appears to be invisible at first sight as the amplitudes of the peaks do not seem to change as a function of S. At a given NBO/T (for example 0.12 for HPG-5-1 and HPG-4-0), the -98.9 ppm peak amplitude seems to decrease with the addition of S.

The possible changes in Al environments have been investigated. The simulations of the ^{27}Al NMR spectra were performed with DMFit software (Massiot et al., 2002) using Czsimple fitting function for $^{\text{IV}}\text{Al}$ and $^{\text{V}}\text{Al}$ and Gaussian function for $^{\text{VI}}\text{Al}$. For An-Di, the different Al species peak position (δ_{iso}) is constant in between the samples at $\sim +64$, $+30$ and 0 ppm for $^{\text{IV}}\text{Al}$, $^{\text{V}}\text{Al}$ and $^{\text{VI}}\text{Al}$, respectively. The derived error on the δ_{iso} values is less than 1% in relative as given by DMFit software. The derived δ_{iso} values are consistent with previous observations (e.g. Stebbins et al., 2000; Neuville et al., 2006). The $^{\text{IV}}\text{Al}$ quadrupolar coupling constant (C_q) is also constant as a function of S at 5.6 MHz, also in agreement with previous findings. The C_q value for $^{\text{V}}\text{Al}$ is lower than for $^{\text{IV}}\text{Al}$ at values between 1 and 2 MHz. This suggests that S and H_2O do not produce significant changes in the Al structural environment in agreement with the observed changes observed in Figure 6 with the difference signal between S-free and S-bearing glasses.

For HPG composition, the δ_{iso} for $^{\text{IV}}\text{Al}$ environment is constant within the samples at $\sim +57.5$ ppm. The C_q value is higher than for An-Di samples suggesting a more distorted environment for $^{\text{IV}}\text{Al}$ in HPG in agreement with the almost fully polymerized nature of this composition.

Overall, our spectral analyses suggest that S has a profound effect on the silicon environments whereas it produces little or no effect on the aluminium environment. In contrast to the suggestion made by Tsujimura et al. (2004), which were however based on more simple compositions, we suggest that S dissolved in silicate melts induces a polymerization of the latter by decreasing the abundances of less polymerized units (Q^2 species) and increasing the abundance of more polymerized units (Q^{4*} and possibly Q^3 species). Currently, it appears difficult to conceal our results with recent EXAFS data.

Recent work by Brendebach et al. (2009) suggests that S dissolves in glass by occupying the void of the glass and therefore not connecting to the silicate network. However, their study is based on a very peculiar alkali- and boron-rich composition (by geological standards). The inferred mechanisms (isolated NaSO_4 clusters) may not be applicable to our studied glass compositions which are analogous to natural compositions and synthesised under pressure.

5.3 *The extent of Si polymerization upon SO_4^{2-} dissolution based on ^{29}Si NMR simulation*

The changes of An-Di melts polymerization as a function of S and compositional changes (expressed by the NBO/T) are represented in Figure 8. The results as a function of S content are shown in Figure 8A. We can see that; under oxidizing conditions, the polymerization is increasing with S content dissolved as SO_4^{2-} : Q^{4*} changes from 18.6% to 25.0% (see Table 3) whereas in parallel the Q^2 abundance decreases from 36.3% to 29.4%. The Q^3 unit abundance shows almost no variation or a slight increase. The determined error on each peak area is on the order of 1% in relative for An-Di (see Table 3). We can also observe that the change in polymerization of the melt is non-monotonic with a large inflexion of the species abundances at around 3000 ppm S. This inflexion is currently not explained.

The change in melt polymerization cannot be explained by the change in composition and OH dissolution mechanism only as the OH influence is taken into account for the NBO/T calculation and the water speciation is similar in between the different An-Di glass samples. We report in Figure 8B the change in Q^n species as a function of the calculated

NBO/T. We can see that the polymerization is higher for samples containing high S content at a given NBO/T. This reinforces our conclusion on the potential effect of S dissolution in silicate melt towards a more polymerized structure with increasing S content. The increase in polymerization is considered to be the result of the S dissolution which induces a clustering of the depolymerized Q^2 -species transforming them into more polymerized unit Q^{4*} . The configuration of this Q^{4*} will be discussed later (see section 5.4).

This polymerization effect of S is only occurring in depolymerized glass An-Di and does not appear to occur in highly polymerized glass HPG. The change in the different Q-species abundances in HPG samples as a function of S content and calculated NBO/T are shown in Figure 9. The abundance of each species remains almost constant as a function of S (Figure 9A) suggesting that negligible changes in the polymerization occur upon S dissolution.

In Figure 9B, we show the Q^n species abundances in the HPG glasses as a function of the calculated NBO/T. We observe that the S-bearing samples exhibit a higher polymerization (if we consider that the lowest Q^n species is assigned to $Q^3(0Al)$) than for S-free samples at a given calculated NBO/T. However, although the error on the Q^n species abundances is low (within the point as reported by Origin[®] software package), we prefer not to draw hasty conclusions on the effect of S in HPG glasses as it is based on only a few samples.

As a strong polymerization effect is induced by the S dissolution in An-Di glass samples, the calculated NBO/T from the major element composition in Table 1 does not reflect the true NBO/T. We have therefore recalculated apparent NBO/Si using measured Q-species

abundances. The value reported in Table 3 is only an approximation value because it does only account for the Si environments (i.e. NBO/Si). The apparent NBO/Si was calculated with the following equation (Eq. 8) as proposed in earlier studies (e.g. Frantz and Mysen, 1995):

$$NBO/Si = 1 \times X Q^3 + 2 \times X Q^2 \quad \text{Eq. 8}$$

where $X Q^n$ is the measured molar fraction of the Q^n species. This equation only considers the silicate framework built by the SiO_4 tetrahedra and does not take into account the framework built by the AlO_4 , AlO_5 or AlO_6 , as identified in An-Di by ^{27}Al NMR. In particular, results obtained by $\{^1H\}$ - ^{27}Al CPMAS NMR (not presented here for clarity) suggest a strong proximity of H atoms and Al atoms in the AlO_6 environments. Hence it is likely that AlO_6 units are not fully polymerized and have a non-negligible content of NBOs. Moreover, AlO_4 species may not be fully polymerized and the existence of AlO_4 in Q^3 configuration is possible as suggested for different kind of compositions (e.g. Zeng et al., 2000; Neuville et al., 2004a, b).

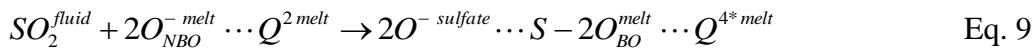
The S-free samples show a higher measured value for the NBO/Si than for the S-bearing samples (Figure 10) in agreement with the polymerization effect of S in An-Di eutectic glasses.

5.4 Dissolution mechanism of S: Possible implications for melt physical properties.

The dissolution of S in An-Di glass induces structural changes which are accompanied by possible changes in melt physical properties such as viscosity. A common view for

aluminosilicate melt is that the increase in polymerization of the melt is correlated with the increase in melt viscosity (McMillan et al., 1994).

Under oxidizing conditions, the dissolution of S atoms provokes the polymerization of the melt. In this section, we propose a potential chemical reaction for S dissolution mechanism explaining the polymerization increase. The fact that less polymerized Q^2 units is decreasing in abundance in favor to the formation of more polymerized Q^4 units suggests that, at some point, SO_4^{2-} species combines with available NBOs in the melt. It is consistent with previous studies suggesting that the S content increases with increasing NBOs (Backneas and Deubener, 2011 and reference therein). Hence, on the basis to Eq. 2 we have rearranged the SO_4^{2-} dissolution reaction so as to include the change in XQ^n :



In Eq. 9, the S dissolution is initiated from the fluid phase in which the initial S reacts with H_2O molecules to form SO_2 , as commonly assumed (Scaillet and Pichavant, 2005). The available SO_2 will dissolve in the melt by consumption of the two available NBOs from the Q^2 species. This linkage produces BO intercalated between S and Si atoms such as $S - 2O^{BO} - Si$. This mechanism is hypothetical and the reaction pathway is likely to be more complicated than a simple reaction. It should be highlighted that the proposed reaction is consistent with our current knowledge of S dissolution mechanism and resembles to Eq. 2; however, Eq. 2 is very simplistic and do not describe the structural changes occurring in the glass structure.

Recent molecular modelling by Machacek et al. (2010) proposed a series of reactions for the S dissolution mechanism in Na_2O - CaO - SiO_2 melts under oxidizing conditions. One step in their molecular modelling involves the formation of $Si - O - S$ linkage. The net

result of the reactions series is to transform the SO_2 molecule in free SO_4 compensated by network modifying cations. A similar mechanism has been suggested by Brendebach et al. (2009) on the basis of X-ray Absorption Spectroscopy. We propose a similar approach but instead of having free SO_4 , the SO_4 molecule will be linked to the silicate framework. In the proposed Eq. 9, we suggest that SO_4^{2-} does not behave as network modifying cluster but instead SO_4^{2-} clusters linked to the silicate network play the role of network former. Hence, we suspect that there is coexistence of two different networks: silicate network and sulphate network. The Eq. 9 is one possible mechanism which has the advantage to explain the observed change in the ^{29}Si NMR spectra.

The consumption of one Q^2 to produce one Q^{4*} is consistent with the observed change in XQ^n shown in Figure 8A. The decrease in Q^2 concentration is compensated by the increase in Q^{4*} concentration whereas the Q^3 concentration remains almost constant.

The modification of the silicate glass polymerization upon S dissolution could produce significant changes on silicate melt viscosity. It is commonly assumed that H_2O dissolves in silicate by breaking Si-O-Si bond inducing a melt depolymerization. This melt depolymerization is accompanied by a decrease in melt viscosity (Dingwell et al., 1996; Romano et al., 2001). Hence, as S induces an increase in polymerization, one would expect S to have the opposite effect on melt viscosity.

It is worth recalling that the present study focuses on glass structure. Thus, the derived structural information represents the structure frozen-in at the glass transition temperature (T_g) and does not represent the true structure of the melt at high-temperature (Brandiss and Stebbins, 1988; Maekawa and Yokokawa, 1997). Besides, the investigated S speciation and dissolution mechanism in glasses might be totally different in the melt at

high temperature as it known for other volatiles such as water (Zhang et al., 1995; Nowak and Behrens, 2001) or carbon dioxide (Morizet et al., 2001; Nowak et al., 2003).

However, the different Q^n speciation as a function of ppm S may indicate that Tg is different in between the glass samples and this presumably could result in the S dissolution. Although the effect of sulphate species on Tg is yet to be proven, one possibility is an increase in Tg as a function of S content dissolved as SO_4^{2-} groups.

6 Summary:

We have conducted an experimental study at high pressure (300 MPa) and high temperature (1250°C) and under highly oxidizing conditions ($\Delta FMQ+3$) so as to investigate the possible effect of S dissolution onto the aluminosilicate, water-bearing, glass structure. Two different starting compositions were chosen for their significant differences in melt structure: HPG which is fully polymerized with NBO/T = 0; An-Di which is slightly depolymerized with NBO/T = 0.921.

The micro-Raman analyses of glasses indicate that S dissolves in both compositions as SO_4^{2-} groups. The presence of SO_4^{2-} groups is in agreement with previous investigations conducted under similar oxidizing conditions.

The S content increases with the amount of S loaded and with increasing NBOs concentration. Therefore, highly depolymerized glass (e.g. nephelinite, melilitite or carbonatite) with high NBO/T will be able to dissolve a large quantity of S. This aspect appears important for future studies on S degassing processes.

Investigation of the different glasses by NMR spectroscopy reveals that the glass structure can be affected by the dissolution of S. The Al environments in both

compositions are not affected by the presence of S whereas the Si environments are modified but only for depolymerized An-Di glasses. HPG glass structure is not changed by the dissolution of S. The net effect of S is to increase the polymerization of An-Di melt. NMR analyses show that the Q^2 species forming a part of the silicate framework combines with SO_4^{2-} groups to form clusters having the spectroscopic signature of Q^4 units, ie more polymerized. The molecular arrangement of this cluster is currently unknown; however we suggest a possible form $S - O - Si$.

We suggest also that the impact of SO_4^{2-} dissolution on slightly depolymerized melt viscosity is opposite to the effect of water. As such, SO_4^{2-} dissolution is likely to increase the melt viscosity. The implications of this possibility for magmatic transport processes should be explored in the future.

Acknowledgments:

The authors are grateful to the University of Orléans, the University of Nantes and the CNRS for their financial support and access to analytical facilities. We also thank Dr. R. Champallier for his technical help. Constructive reviews by Roberto Moretti and an anonymous reviewer greatly improved the quality of the manuscript.

References:

Ahmed, A.A., Sharaf, N.A., Condrate, R.A.S., 1997. Raman microprobe investigation of sulphur-doped alkali borate glasses. *J. Non-Cryst. Solids* 210, 59-69.

Backnaes, L., Deubener, J., 2011. Experimental studies on sulfur solubility in silicate melts at near-atmospheric pressure. In: H. Behrens and J.D. Webster (eds.) *Sulfur in magmas and melts: Its importance for natural and technical processes*. Washington, Mineralogical Society of America, Geochemical Society, *Rev. Mineral. Geochem.* 73, 143-165.

Baker, D.R., Moretti, R., 2011. Modeling the solubility of sulfur in magmas: a 50-year old geochemical challenge. In: H. Behrens and J.D. Webster (eds.) *Sulfur in magmas and melts: Its importance for natural and technical processes*. Washington, Mineralogical Society of America, Geochemical Society, *Rev. Mineral. Geochem.* 73, 167-213.

Beermann, O., Botcharnikov, R.E., Holtz, F., Diedrich, O., Nowak, M., 2011. Temperature dependence of sulfide and sulfate solubility in olivine-saturated basaltic magmas. *Geochim. Cosmochim. Acta* 75, 7612-7631.

Begaudeau, K., Morizet, Y., Florian, P., Paris, M., Mercier, J.-C., 2012. Solid-state NMR analyses of Fe-bearing minerals: implications and application for Earth sciences. *Eur. Journal Min.* 24, 535-550.

Behrens, H., Romano, C., Nowak, M., Holtz, F., Dingwell, D.B., 1996. Near-infrared spectroscopic determination of water species in glasses of the system MAlSi_3O_8 (M = Li, Na, K) : an interlaboratory study. *Chem. Geol.* 128, 41-63.

Brandiss, M.E., Stebbins, J.F., 1988. Effects of T on the structures of silicate liquids: ^{29}Si NMR results. *Geochim. Cosmochim. Acta* 52, 2659-2669.

Brendebach, B., Denecke, M.A., Roth, G., Weisenburger, S., 2009. Sulfur incorporation in high level nuclear waste glass: a S K-edge XAFS investigation. *J. Phys. Conf. Ser.* 190, 012186.

Carroll, M.R., Rutherford, M.J., 1988. Sulfur speciation in hydrous experimental glasses of varying oxidation state: Results from measured wavelength shifts of sulfur X-rays. *Am. Mineral.* 73, 845-849.

Carroll, M.R., Webster, J.D., 1994. Solubilities of sulfur, noble gases, nitrogen, chlorine, and fluorine in magmas. In: J.R. Holloway and M.R. Carroll. (eds.) *Volatiles in Magmas*. Washington, Mineralogical Society of America, Geochemical Society. 30, pp. 231-280.

Chivers, T., Gilmour, E., Kydd, R.A., 1978. Vibrational spectra of sulphur-doped borate glasses. *J. Mat. Sci.* 13, 1585-1588.

Clemente, B., Scaillet, B., Pichavant, M., 2004. The solubility of sulphur in hydrous rhyolitic melts. *J. Petrol.* 45(11), 2171-2196.

Cody, G.D., Mysen, B.O., Lee, S.K., 2005. Structure vs. composition: A solid-state ^1H and ^{29}Si NMR study of quenched glasses along the Na_2O - SiO_2 - H_2O join. *Geochim. Cosmochim. Acta* 69(9), 2373-2384.

Di Carlo, I., Pichavant, M., Rotolo, S.G., Scaillet, B., 2006. Experimental crystallization of a high-K arc basalt: The golden pumice, Stromboli volcano (Italy). *J. Petrol.* 47, 1317-1343.

Dingwell, D.B., Romano, C., Hess, K.-U., 1996. The effect of water on the viscosity of a haplogranitic melt under P-T-X conditions relevant to silicic volcanism. *Contrib. Mineral. Petrol.* 124, 19-28.

Dreibus, G., Palme, H., 1996. Cosmochemical constraints on the sulfur content in the Earth's core. *Geochim. Cosmochim. Acta* 60, 1125-1130.

Dixon, J.E., Stolper, E.M., Holloway, J.R., 1995. An experimental study of water and carbon dioxide solubilities in Mid-Ocean Ridge Basaltic liquids. Part I: calibration and solubility models. *J. Petrol.* 36, 1607–1631.

Emerson, J.F., Stallworth, P.E., Bray, P.J., 1989. High-field ^{29}Si NMR studies of alkali silicate glasses. *J. Non Cryst. Solids* 113, 253-259.

Farnan, I., Kohn, S.C., Dupree, R., 1987. A study of the structural role of water in hydrous silica glass using Cross-Polarization Magic Angle Spinning NMR. *Geochim. Cosmochim. Acta* 51, 2869-2873.

Farnan, I., Stebbins, J.F., 1994. The nature of the glass transition in a silica-rich oxide melt. *Science* 265, 1206-1209.

Fincham, C.J.B., Richardson, F.D., 1954. The behavior of sulphur in silicate and aluminate melts. *Proc. R. Soc. Lond. A* 223, 40-62.

Fleet, M.E., 2005. XANES spectroscopy of sulfur in Earth materials. *Can. Mineral.* 43, 1811-1838.

Frantz, J.D., Mysen, B.O., 1995. Raman spectra and structure of BaO-SiO_2 , SrO-SiO_2 and CaO-SiO_2 melts to 1600°C . *Chem. Geol.* 121, 155-176.

Freda, C., Baker, D.R., Scarlato, P., 2005. Sulfur diffusion in basaltic melts. *Geochim. Cosmochim. Acta* 69, 5061-5069.

Gaillard, F., Scaillet, B., 2009. The sulfur content of volcanic gases on Mars. *Earth Planet. Science Lett.* 279, 34-43.

Gaillard, F., Scaillet, B., Arndt, N., 2011. Atmospheric oxygenation caused by a change in volcanic degassing pressure. *Nature* 478, 229-232.

Gaillard, F., Michalski, J., Berger, G., McLennan, S.M., Scaillet, B., 2013. Geochemical reservoirs and timing of sulfur cycling on Mars. *Space Sci. Rev.* 174, 251-300.

Giggenbach, W.F., 1980. Geothermal gas equilibria. *Geochim. Cosmochim. Acta* 44, 2021-2032.

Giggenbach, W.F., 1987. Redox processes governing the chemistry of fumarolic gas discharges from White Island, New Zealand. *Appl. Geochem.* 2, 143-161.

Grimmer, A.R., Magi, M., Hähnert, M., Stade, H., Samoson, A., Wieker, W., Lippmaa, E., 1984. High resolution solid state ^{29}Si NMR spectroscopic studies of binary alkali silicate glasses. *Phys. Chem. Glasses* 25(4), 105-109.

Haughton, D.R., Roeder, P.L., Skinner, B.J., 1974. Solubility of sulfur in mafic magmas. *Econ. Geol.* 69, 451-467.

Holzheid, A., Grove, T.L., 2002. Sulfur saturation limits in silicate melts and their implications for core formation scenarios for terrestrial planets. *Am. Mineral.* 87, 227-237.

Iacono-Marziano, G., Gaillard, F. Pichavant, M., 2008. Limestone assimilation by basaltic magmas: an experimental re-assessment and application to Italian volcanoes. *Contrib. Mineral. Petrol.* 155, 719-738.

Iacono-Marziano, G., Morizet, Y., Le Trong, E., Gaillard, F., (2012) New experimental data and semi-empirical parameterization of H₂O-CO₂ solubility in mafic melts. *Geochim. Cosmochim. Acta* 97, 1-23..

Jugo, P.J., Luth, R.W., Richards, J.P., 2005a. An experimental study of the sulfur content in basaltic melts saturated with immiscible sulfide or sulfate liquids at 1300°C and 1.0 GPa. *J. Petrol.* 46(4), 783-798.

Jugo, P.J., Luth, R.W., Richards, J.P., 2005b. Experimental data on the speciation of sulfur as a function of oxygen fugacity in basaltic melts. *Geochim. Cosmochim. Acta* 69, 497-503.

Jugo, P.J., Wilke, M., Botcharnikov, R.E., 2010. Sulfur K-edge XANES analysis of natural and synthetic basaltic glasses: Implications for S speciation and S content as function of oxygen fugacity. *Geochim. Cosmochim. Acta* 74, 5926-5938.

Klimm, K., Botcharnikov, R.E., 2010. The determination of sulfate and sulfide species in hydrous silicate glasses using Raman spectroscopy. *Am. Mineral.* 95, 1574-1579.

Klimm, K., Kohn, S.C., O'Dell, L.A., Botcharnikov, R.E., Smith, M.E., 2012a. The dissolution mechanism of sulphur in hydrous silicate melts. I: Assessment of analytical techniques in determining the sulphur speciation in iron-free to iron-poor glasses. *Chem. Geol.* **322-323**, 237-249

Klimm, K., Kohn, S.C., Botcharnikov, R.E., 2012b. The dissolution mechanism of sulphur in hydrous silicate melts. II: Solubility and speciation of sulphur in hydrous silicate melts as a function of fO_2 . *Chem. Geol.* 322-323, 250-267.

Kohn, S.C., Dupree, R., Smith, M.E., 1989. A multi-nuclear magnetic-resonance study of the structure of hydrous albite glasses. *Geochim. Cosmochim. Acta* 53, 2925–2935.

Kummerlen, J., Merwin, L.H., Sebal, A., Keppler, H., 1992. Structural role of H_2O in sodium silicate glasses: results from ^{29}Si and 1H NMR spectroscopy. *J. Phys. Chem.* 96, 6405-6410.

Lange, R.A., Carmichael, I.S.E., 1987. Densities of Na_2O - K_2O - CaO - MgO - FeO - Fe_2O_3 - Al_2O_3 - TiO_2 - SiO_2 liquids: new measurements and derived partial molar properties. *Geochim. Cosmochim. Acta* 53, 2195-2204.

Laws, D.D., Bitter, H.-M.L., Jerschow, A., 2002. Solid State NMR spectroscopic methods in Chemistry. *Ange. Chem. Int. Ed.* 41, 3096-3129.

Lenoir, M., Grandjean, A., Poissonnet, S., Neuville, D.R., 2009. Quantitation of sulfate solubility in borosilicate glasses using Raman spectroscopy. *J. Non-Cryst. Solids* 355, 1468-1473.

Lesne, P., Scaillet, B., Pichavant, M., Beny, J.-M., 2011. The carbon dioxide solubility in alkali basalts: an experimental study. *Contrib. Mineral. Petrol.* 162, 153-168.

Lippmaa, E., Mägi, M., Samoson, A., Engelhardt, G., Grimmer, A.-R., 1979. Structural studies of silicates by Solid-State high-resolution ^{29}Si NMR. *J. Am. Chem. Soc.* 102, 4889-4893.

Liu, Y., Samaha, N.-T., Baker, D.R., 2007. Sulfur concentration at sulfide saturation (SCSS) in magmatic silicate melts. *Geochim. Cosmochim. Acta* 71, 1783-1799.

Machacek, J., Gedeon, O., Liska, M., Marhoul, F., 2010. Molecular simulations of silicate melts doped with sulphur and nitrogen. *J. Non-Cryst. Solids* 356, 2458-2464.

Maekawa, H., Maekawa, T., Kawamura, S., Yokokawa, T., 1991. The structural groups of alkali silicate glasses determined from ^{29}Si MAS-NMR. *J. Non-Cryst. Solids* 127, 53-64.

Maekawa, H., Yokokawa, T., 1997. Effects of temperature on silicate melt structure: A high temperature ^{29}Si NMR study of $\text{Na}_2\text{Si}_2\text{O}_5$. *Geochim. Cosmochim. Acta* 61, 2569-2575

Malfait, W.J., Halter, W.E., Morizet, Y., Meier, B.H., Verel, R., 2007. Structural control on bulk melt properties: Single and double quantum ^{29}Si NMR spectroscopy on alkali-silicate glasses. *Geochim. Cosmochim. Acta* 71, 6002-6018.

Malfait, W.J., Verel, R., Ardia, P., Sanchez-Valle, C., 2012. Aluminium coordination in rhyolite and andesite glasses and melts: Effect of temperature, pressure, composition and water content. *Geochim. Cosmochim. Acta* 77, 11-26.

Mandeville, C.W., Webster, J.D., Rutherford, M.J., Taylor, B.E., Timbal, A., Faure, K., 2002. Determination of molar absorptivities for infrared absorption bands of H_2O in andesitic glasses. *Am. Mineral.* 87, 813-821.

Massiot, D., Fayon, F., Capron, M., King, I., Le Calvé, S., Alonso, B., Durand, J.O., Bujoli, B., Gan, Z., Hoatson, G., 2002. Modelling one and two-dimensional solid-state NMR spectra. *Magn. Res. Chem.* 40, 70-76.

McDonough, W.F., Sun, S.-s, 1995. The composition of the Earth. *Chem. Geol.* 120, 223-253.

McMillan, P.F., Poe, B.T., Gillet, P., Reynard, B., 1994. A study of SiO₂ glass and supercooled liquid to 1950 K via a high-temperature Raman spectroscopy. *Geochim. Cosmochim. Acta* 58(17), 3653-3664.

Merzbacher, C.I., Sherriff, B.L., Hartman, J.S., White, W.B., 1990. A high-resolution ²⁹Si and ²⁷Al NMR study of alkaline earth aluminosilicate glasses. *J. Non-Cryst. Solids* 124, 194-206.

Métrich, N., Clocchiatti, R., 1996. Sulfur abundance and its speciation in oxidized alkaline melts. *Geochim. Cosmochim. Acta* 60(21), 4151-4160.

Métrich, N., Mandeville, C.W., 2010. Sulfur in magmas. *Elements* 6, 81-86.

Moretti, R., Ottonello, G., 2005. Solubility and speciation of sulfur in silicate melts: The Conjugated Toop-Samis-Flood-Grjotheim (CTSFG) model. *Geochim. Cosmochim. Acta* 69, 801-823.

Morizet, Y., Kohn, S.C., Brooker, R.A., 2001. Annealing experiments on CO₂-bearing jadeite glass: an insight into the true temperature dependence of CO₂ speciation in silicate melts. *Min. Mag.* 65, 701-707.

Morizet, Y., Paris, M., Gaillard, F., Scaillet, B., 2009. Raman quantification factor calibration for CO-CO₂ gas mixture in synthetic fluid inclusions: Application to oxygen fugacity calculation in magmatic systems. *Chem. Geol.* 264, 58-70.

Morizet, Y., Paris, M., Gaillard, F., Scaillet, B., 2010. C-O-H fluid solubility in haplobasalt under reducing conditions: An experimental study. *Chem. Geol.* 279, 1-16.

Moune, S., Holtz, F., Botcharnikov, R.E., 2009. Sulphur solubility in andesitic to basaltic melts: Implications for Hekla volcano. *Contrib. Mineral. Petrol.* 157, 691-707.

Mysen, B.O., 1988. Structure and properties of silicate melts. In: *Development in Geochemistry*, vol. 4. Elsevier, Amsterdam, 354 pp.

Mysen, B.O., 1990. Effect of pressure, temperature and bulk composition on the structure and species distribution in depolymerised alkali aluminosilicate melts and quenched melts. *J. Geophys. Res. B* 95, 15733-15744.

Mysen, B.O., Frantz, J.D., 1993. Structure and properties of alkali silicate melts at magmatic temperature. *Eur. J. Min.* 5, 393-407.

Mysen, B.O., Richet, P., 2005. Silicate glasses and melts: Properties and structure. pp. 560.

Mysen, B.O., 1999. Structure and properties of magmatic liquids: From haplobasalt to haploandesite. *Geochim. Cosmochim. Acta* 63(1), 95-112.

Mysen, B.O., 1998. Transport and configurational properties of silicate melts: Relationship to melt structure at magmatic temperatures. *Phys. Earth Planet. Int.* 107, 23-32.

Neuville, D.R., Cormier, L., Flank, A.M., Briois, V., Massiot, D., 2004a. Al speciation and Ca environment in calcium aluminosilicate glasses and crystals by Al and Ca K-edge X-ray absorption spectroscopy. *Chem. Geol.* 213, 153–163.

Neuville, D.R., Cormier, L., Massiot, D., 2004b. Al environment in tectosilicate and peraluminous glasses: a ^{27}Al MQMAS NMR, Raman, and XANES investigation. *Geochim. Cosmochim. Acta* 68, 5071–5079.

Neuville, D.R., Cormier, L., Massiot, D., 2006. Al coordination and speciation in calcium aluminosilicate glasses: Effects of composition determined by ^{27}Al MQ-MAS NMR and Raman spectroscopy. *Chem. Geol.* 229, 173-185.

Neuville, D.R., 2006. Viscosity, structure and mixing in (Ca, Na) silicate melts. *Chem. Geol.* 229, 28-41.

Newman, S., Lowenstern, J.B., 2002. VolatileCalc: a silicate melt-H₂O-CO₂ solution model written in Visual Basic for excel. *Comp. Geosc.* 28, 597-604.

Nowak, M., Behrens, H., 2001. Water in rhyolitic magmas: getting a grip on a slippery problem. *Earth Planet. Sci. Lett.* 184, 515-522.

Nowak, M., Porbatzki, D., Spickenbom, K., Diedrich, O., 2003. Carbon dioxide speciation in silicate melts: a restart. *Earth Planet. Sci. Lett.* 207, 131-139.

O'Neill, H.S.C., Mavrogenes, J.A., 2002. The sulfide capacity and the sulfur content at sulfide saturation of silicate melts at 1400°C and 1 bar. *J. Petrol.* 43, 1049-1087.

Oppenheimer, C., Scaillet, B., Martin, R.S., 2011. Sulfur degassing from volcanoes: source conditions, surveillance, plume chemistry and Earth system impacts. *Sulfur in magmas and melts: Its importance for natural and technical processes.* H. Behrens and J. D. Webster. Washington, Mineralogical Society of America, Geochemical Society. 73, 363-421.

Padro, D., Schmidt, B.C., Dupree, R., 2003. Water solubility mechanism in hydrous aluminosilicate glasses: Information from ^{27}Al MAS and MQMAS NMR. *Geochim. Cosmochim. Acta* 67(8), 1543-1551.

Paris, E., Giuli, G., Carroll, M.R., Davoli, I., 2001. The valence and speciation of sulfur in glasses by X-ray absorption spectroscopy. *Can. Mineral.* 39, 331-339.

Pichavant, M., Di Carlo, I., Le Gac, Y., Rotolo, S., Scaillet, B., 2009. The deep feeding system of basaltic volcanoes: experimental evidence from Stromboli (Italy). *J. Petrol.* 50, 601-624.

Pokrovski, G.S., Dubrovinsky, L.S., 2011. The S_3^- ion is stable in geological fluids at elevated temperatures and pressures. *Science* 331, 1052-1054.

Pradel, A., Taillades, G., Ribes, M., Eckert, H., 1995. ^{29}Si NMR structural studies of ionically conductive silicon chalcogenide glasses and model compounds. *J. Non-Cryst. Solids* 188, 75-86.

Prouteau, G., Scaillet, B., 2013. Experimental constraints on sulphur behaviour in subduction zones: Implications for TTG/Adakite production and the global sulphur cycle since the Archean. *J. Petrol.* 54, 183-213.

Robert, E., Whittington, A., Fayon, F., Pichavant, M., Massiot, D., 2001. Structural characterization of water-bearing silicate and aluminosilicate glasses by high-resolution solid state NMR. *Chem. Geol.* 174, 291-305.

Romano, C., Poe, B., Mincione, V., Hess, K.-U., Dingwell, D.B., 2001. The viscosities of dry and hydrous $X\text{AlSi}_3\text{O}_8$ ($X = \text{Li}, \text{Na}, \text{K}, \text{Ca}_{0.5}, \text{Mg}_{0.5}$) melts. *Chem. Geol.* 174, 115-132.

Scaillet, B., Pichavant, M., Roux, J., Humbert, G., Lefèvre, A., 1992. Improvements of the Shaw membrane technique for measurement and control of $f\text{H}_2$ at high temperatures and pressures. *Am. Mineral.* 77, 647-655.

Scaillet, B., Luhr, J.F., Carroll, M.C., 2003. Petrological and volcanological constraints on volcanic sulphur emissions to the atmosphere. *Volcanism and the Earth's atmosphere*. A. Robock and C. Oppenheimer. *Geophys. Mono.* 139, 11-40.

Scaillet, B. Pichavant, M., 2005. A model of sulphur solubility for hydrous mafic melts: application to the determination of magmatic fluid compositions of Italian volcanoes. *Ann. Geophys.* 48(4/5), 671-697.

Schmidt, B.C., Holtz, F., Pichavant, M., 1999. Water solubility in haplogranitic melts coexisting with H_2O - H_2 fluids. *Contrib. Mineral. Petrol.* 136, 213-224.

Schmidt, B.C., Riemer, T., Kohn, S.C., Behrens, H., Dupree, R., 2000. Different water solubility mechanisms in hydrous glasses along the Qz-Ab join: Evidence from NMR spectroscopy. *Geochim. Cosmochim. Acta* 64(3), 513-526.

Schmidt, B.C., Riemer, T., Kohn, S.C., Holtz, F., Dupree, R., 2001. Structural implications of water dissolution in haplogranitic glasses from NMR spectroscopy: influence of total water content and mixed alkali effect. *Geochim. Cosmochim. Acta* 65(17), 2949-2964.

Schneider, J., Mastelaro, V.R., Zanutto, E.D., Shakhmatkin, B.A., Vedishcheva, N.M., Wright, A.C., Panepucci, H., 2003. Q^n distribution in stoichiometric silicate glasses: thermodynamic calculations and ^{29}Si high resolution NMR measurements. *J. Non-Cryst. Solids* 325, 164-178.

Schramm, C.M., De Jong, B.H.W.S., Parziale, V.E., 1984. ^{29}Si Magic Angle Spinning NMR study on local silicon environments in amorphous and crystalline lithium silicates. *J. Am. Chem. Soc.* 106, 4396-4402.

Shannon, R.D., Prewitt, C.T., 1969. Effective ionic radii in oxides and fluorides. *Acta Crystallogr. B* 25, 925-946.

Smith, K.A., Kirkpatrick, R.J., Oldfield, E., Henderson, D.M., 1983. High-resolution silicon-29 nuclear magnetic resonance spectroscopic study of rock-forming silicates. *Am. Mineral.* 68, 1206-1215.

Stebbins, J.F., 1995. Dynamics and structure of silicate and oxide melts: Nuclear Magnetic Resonance studies. J.F. Stebbins, P.F. McMillan and D.B. Dingwell. Washington, Mineralogical Society of America, Geochemical Society. 32, 190-246.

Stebbins, J.F.; Kroeker, S., Lee, S.K., Kiczinski, T.J., 2000. Quantification of 5 and 6-coordinated Al ions in aluminosilicate and fluoride containing glasses by high field, high resolution ^{27}Al NMR. *J. Non-Cryst. Solids* 275, 1-6.

Stebbins, J.F., Dubinsky, E.V., Kanehashi, K., Kelsey, K.E., 2008. Temperature effects on non-bridging oxygen and aluminium coordination number in calcium aluminosilicate glasses and melts. *Geochim. Cosmochim. Acta* 72, 910-925.

Stelling, J., Behrens, H., Wilke, M., Göttlicher, J., Chalmin-Aljanabi, E., 2011. Interaction between sulphide and H_2O in silicate melts. *Geochim. Cosmochim. Acta* 75, 3542-3557.

Stolper, E.M., 1982. Water in silicate glasses: an infrared spectroscopic study. *Contrib. Mineral. Petrol.* 81, 1-17.

Sykes, D., Kubicki, J.D., Farrar, T., 1997. Molecular orbital calculation of ^{27}Al and ^{29}Si NMR parameters in Q^3 and Q^4 aluminosilicate molecules and implications for the interpretation of hydrous aluminosilicate glass NMR spectra. *J. Phys. Chem. A* 101, 2715-2722.

Taylor, M., Brown, Jr., G.E., 1979. Structure of mineral glasses—I. The feldspar glasses $\text{NaAlSi}_3\text{O}_8$, KAlSi_3O_8 , $\text{CaAl}_2\text{Si}_2\text{O}_8$. *Geochim. Cosmochim. Acta* 43, 61–75.

Toplis, M.J., Kohn, S.C., Smith, M.E., Poplett, I.J.F., 2000. Fivefold-coordinated aluminium in tectosilicate glasses observed by triple quantum MAS NMR. *Am. Mineral.* 85, 1556-1560.

Tsujimura, T., Xue, X., Kanzaki, M., Walter, M.J., 2004. Sulfur speciation and network structural changes in sodium silicate glasses: Constraints from NMR and Raman spectroscopy. *Geochim. Cosmochim. Acta* 68(24), 5081-5101.

Watson, E.B., 1994. Diffusion in volatile-bearing magmas. In: J.R. Holloway and M.R. Carroll. (eds.) *Volatiles in Magmas*. Washington, Mineralogical Society of America, Geochemical Society. 30, 371-411.

White, S.N., 2009. Laser Raman spectroscopy as a technique for identification of seafloor hydrothermal and cold seep minerals. *Chem. Geol.* 259, 240-252.

Wilke, M., Jugo, P.J., Klimm, K., Susini, J., Botcharnikov, R., Kohn, S.C., Janousch, M., 2008. The origin of S⁴⁺ detected in silicate glasses by XANES. *Am. Mineral.* 93, 235-240.

Wilke, M., Klimm, K., Kohn, S.C., 2011. Spectroscopic studies on sulfur speciation in synthetic and natural glasses. In: H. Behrens and J.D. Webster (eds.) *Sulfur in magmas and melts: Its importance for natural and technical processes*. Washington, Mineralogical Society of America, Geochemical Society, *Rev. Mineral. Geochem.* 73, 41-78.

Winther, K.T., Watson, E.B., Korenowski, G.M., 1998. Magmatic sulfur compounds and sulfur diffusion in albite melt at 1 GPa and 1300-1500°C. *Am. Mineral.* 83, 1141-1151.

Withers, A.C., Berhens, H., 1999. Temperature-induced changes in the NIR spectra of hydrous albitic and rhyolitic glasses between 300 and 100 K. *Phys. Chem. Minerals* 27, 119-132.

Xue, X., Kanzaki, M., 2004. Dissolution mechanisms of water in depolymerized silicate melts: Constraints from ¹H and ²⁹Si NMR spectroscopy and ab initio calculations. *Geochim. Cosmochim. Acta* 68, 5027-5057.

Xue, X., Kanzaki, M., 2008. Structure of hydrous aluminosilicate glasses along the diopside-anorthite join: A comprehensive one- and two-dimensional ¹H and ²⁷Al NMR study. *Geochim. Cosmochim. Acta* 72, 2331-2348.

Xue, X., 2009. Water speciation in hydrous silicate and aluminosilicate glasses: Direct evidence from ^{29}Si - ^1H and ^{27}Al - ^1H double-resonance NMR. *Am. Mineral.* 94, 395-398.

Zajacz, Z., Candela, P.A., Piccoli, P.M., Sanchez-Valle, C., 2012. The partitioning of sulfur and chlorine between andesite melts and magmatic volatiles and the exchange coefficients of major cations. *Geochim. Cosmochim. Acta* 89, 81-101.

Zeng, Q., Nekvasil, H., Grey, C.P., 1999. Proton environments in hydrous aluminosilicate glasses: A ^1H MAS, $^1\text{H}/^{27}\text{Al}$, and $^1\text{H}/^{23}\text{Na}$ TRAPDOR NMR study. *J. Phys. Chem. B* 103, 7406-7415.

Zeng, Q., Nekvasil, H., Grey, C.P., 2000. In support of a depolymerization model for water in sodium aluminosilicate glasses: Information from NMR spectroscopy. *Geochim. Cosmochim. Acta* 64, 883-896.

Zhang, P., Grandinetti, P.J., Stebbins, J.F., 1997. Anionic species determination in CaSiO_3 glass using two-dimensional ^{29}Si NMR. *J. Phys. Chem.* 101, 4004-4008.

Zhang, Y., 2010. Diffusion in minerals and melts: theoretical background. *Rev. Mineral. Geochem.* 72, 5-59.

Zhang, Y., Stolper, E.M., Ihinger, P.D., 1995. Kinetics of the reaction $\text{H}_2\text{O} + \text{O} = 2\text{OH}$ in rhyolitic and albitic glasses: Preliminary results. *Am. Mineral.* 80, 593-612.

Figure captions:

Figure 1: Sulphur (S) solubility measured by EPMA for glasses and represented as a function of initial loaded S content during the experiments: A) for An-Di glasses and B) for HPG glasses. The open symbols represent the S solubility measured for different glass chips in different EPMA session (see Table 2). The filled symbols represent the average considered S solubility. The $\text{H}_2\text{O}^{\text{tot}}$ in wt.% is indicated next to each point. The error bars on each open symbol is the standard deviation obtained from EPMA analyses (at least 20). The error bars on filled symbols are the standard deviation calculated from open symbols.

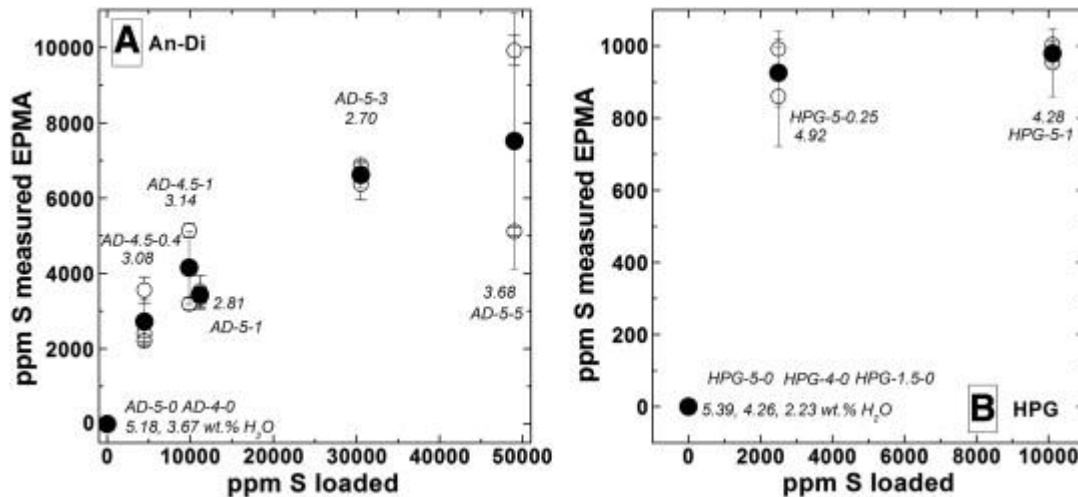


Figure 2: A) Changes in S content in An-Di glass samples as a function of molar $\text{MgO} / \text{MgO} + \text{CaO}$. The open symbols represent the data point acquired for S-free H_2O -bearing samples and the filled symbols are for the S- H_2O -bearing glass samples. B) The same data points are reported as a function of molar $\text{Al}_2\text{O}_3 / \text{Al}_2\text{O}_3 + \text{SiO}_2$. The error reported for this ratio is calculated from conventional error propagation calculation from the error in wt.% obtained by EPMA analyses.

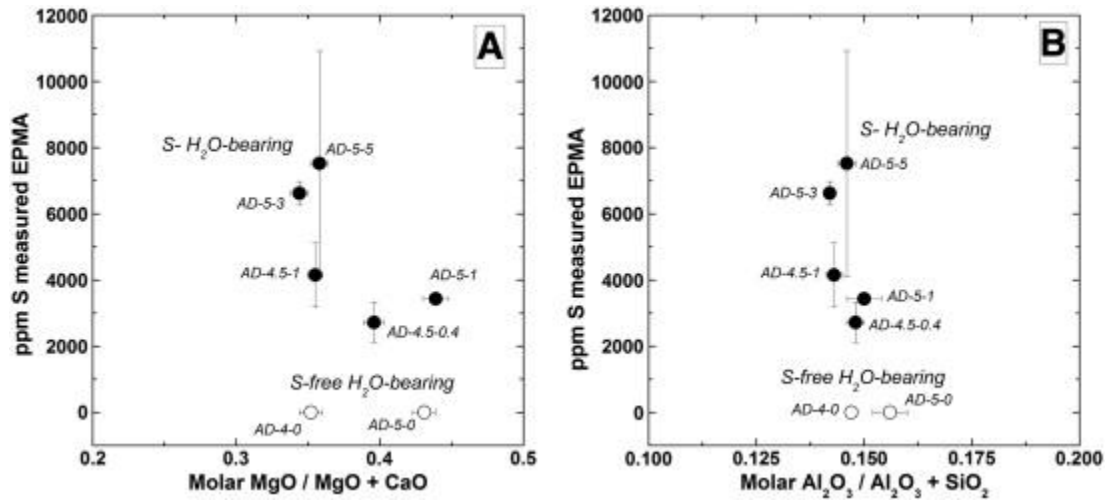


Figure 3: ppm S versus Calculated NBO/T as measured by EPMA. The NBO/T calculation takes into account the effect of water by considering that all dissolved OH groups act as a network modifying cation. Two different set of samples are represented: open symbol for S-free H₂O-bearing samples; filled symbols for S- H₂O-bearing sample.

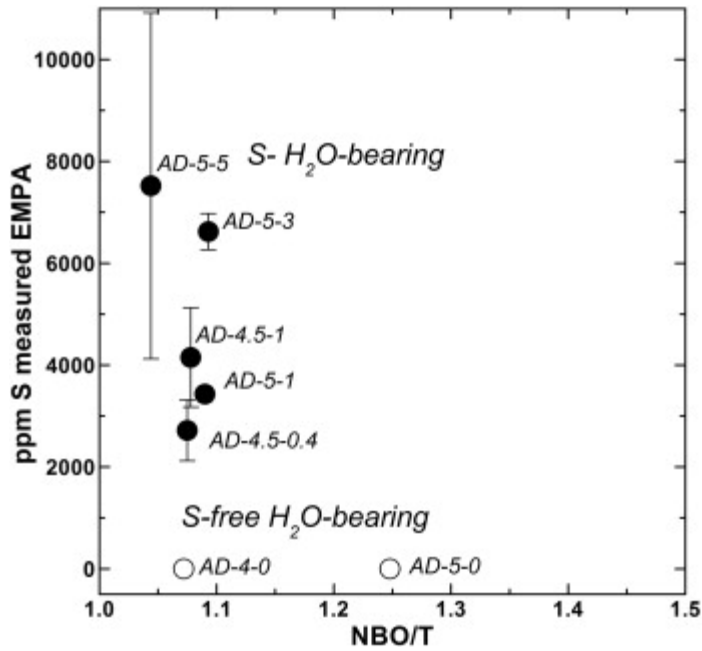


Figure 4: Micro-Raman spectra obtained for several An-Di glass samples and HPG glass samples. A) Spectra obtained for An-Di glasses AD-5-0 (S-free H₂O-bearing) and AD-5-5 (S- H₂O-bearing). A typical spectrum of gypsum (CaSO₄.2H₂O) from the RUFF© database is also reported. The AD-5-5 spectrum shows several peaks indicative of the presence of sulfates dissolved in the glass: 997 cm⁻¹. The possible molecular assignment of the peak at 532 cm⁻¹ is currently uncertain. B) Spectra obtained for HPG glasses HPG-5-0 (S-free H₂O-bearing) and HPG-5-1 (S- H₂O-bearing). Both spectra are similar consistent with the low S solubility in HPG melt. We provide additional Raman spectra in the Supplementary material showing HS groups signature in glasses as well as spectra from fluid inclusions analyses.

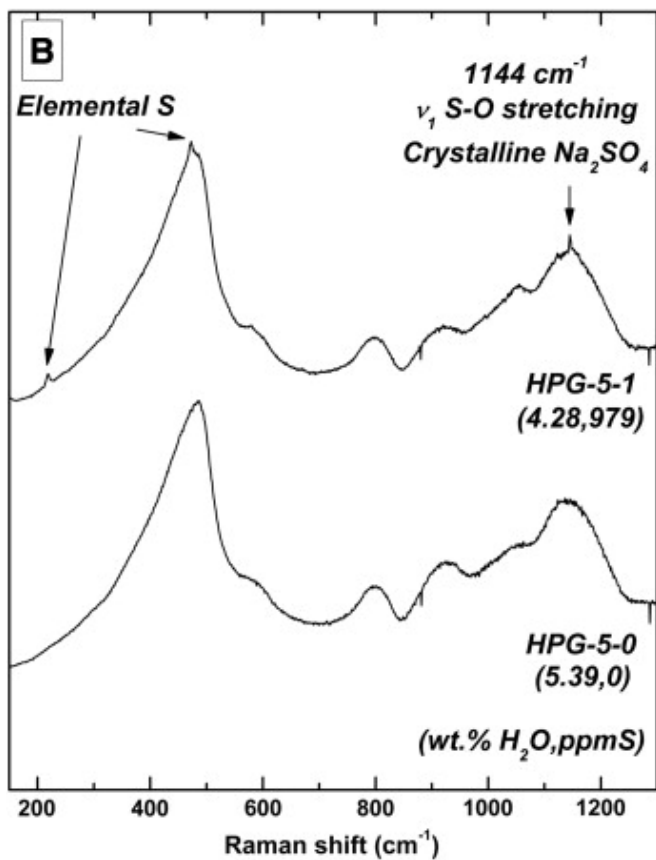
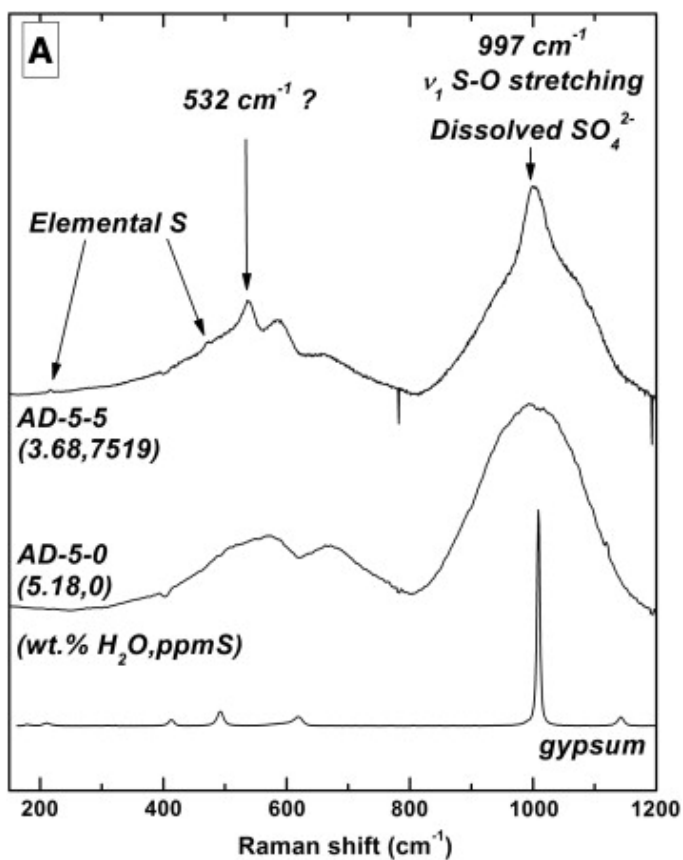


Figure 5: ^{29}Si NMR spectra acquired with single pulse sequence for glass samples. The peak maximum, the ppm S and calculated NBO/T or the wt.% MgO measured by EPMA are indicated next to each spectrum. A) An-Di samples. We observe a shift in the peak maximum from ~ -83 to -86 ppm with increasing S content. B) HPG samples. The peak maximum remains constant with increasing S content at -104 ppm. Additional $\{^1\text{H}\}\text{-}^{29}\text{Si}$ CPMAS spectra are also shown suggesting the existence of several Q^n units under the ^{29}Si envelope. C) An-Di with Various MgO content. The peak maximum is shift from ~ -85 to -83 ppm with increasing MgO content.

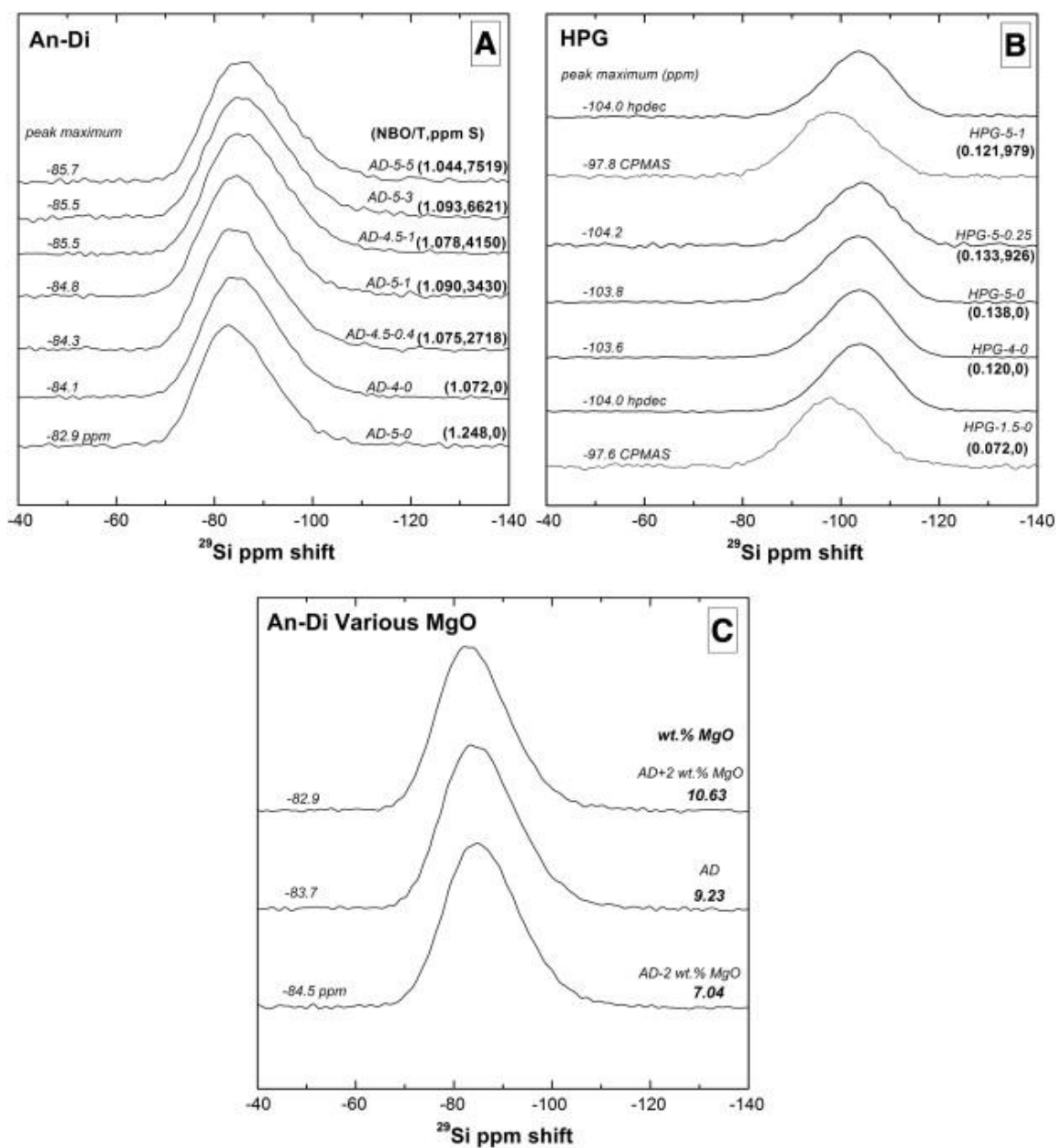


Figure 6: ^{27}Al NMR spectra acquired for glass samples. The different suspected Al species (4-, 5- and 6-coordinated) are shown in each plot. The peak maximum, the ppm S and the calculated NBO/T or the wt.% MgO measured by EPMA are indicated next to each spectrum. A) An-Di samples. Each spectrum is characterized by the presence of $^{\text{IV}}\text{Al}$ mainly and possibly $^{\text{V}}\text{Al}$ and $^{\text{VI}}\text{Al}$ species. The peak maximum is located at $\sim +55$ ppm and

does not seem to be affected by the presence of S. B) HPG samples. Only ^{IV}Al is present in this composition and S does not change the position of the peak.

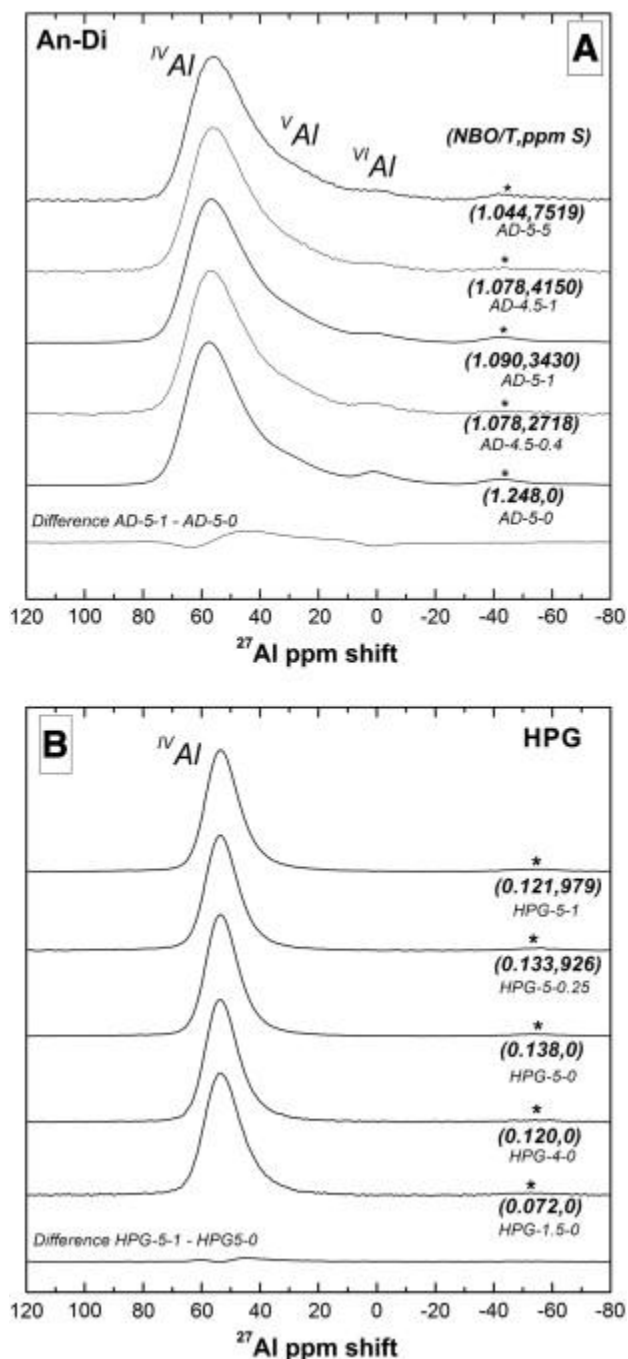


Figure 7: ^{29}Si NMR simulation for An-Di (A) and HPG (B) glass samples. For each sample, the amount of S and the calculated NBO/T is indicated. The dotted line represents the NMR spectrum; the red solid line is the simulated NMR spectrum. The

spectra were simulated with three individual Gaussian peaks for An-Di. For An-Di glass, the derived chemical shift (δ_{iso}) is -79.9, -86.8 and -95.3 ppm for a possible assignment to Q^2 , Q^3 and Q^4 or Q^{4*} , respectively. For HPG, the simulation was performed with only two Gaussian peaks and the assignment was made considering that the proximity of Al atoms induces a shift in the δ_{iso} . The derived δ_{iso} is -105.3 and -98.9 ppm with a possible assignment to $Q^4(0\text{Al})$, $Q^4(1\text{Al})$ or $Q^3(0\text{Al})$, respectively. For all spectra of a given glass composition, the simulation was conducted simultaneously on the entire dataset. For An-Di glass spectrum, there is a clear change in the abundance of the Q-species at -79.9 and -95.3 ppm as a function of ppm S. For HPG glass spectrum, no major change is observed as a function of S.

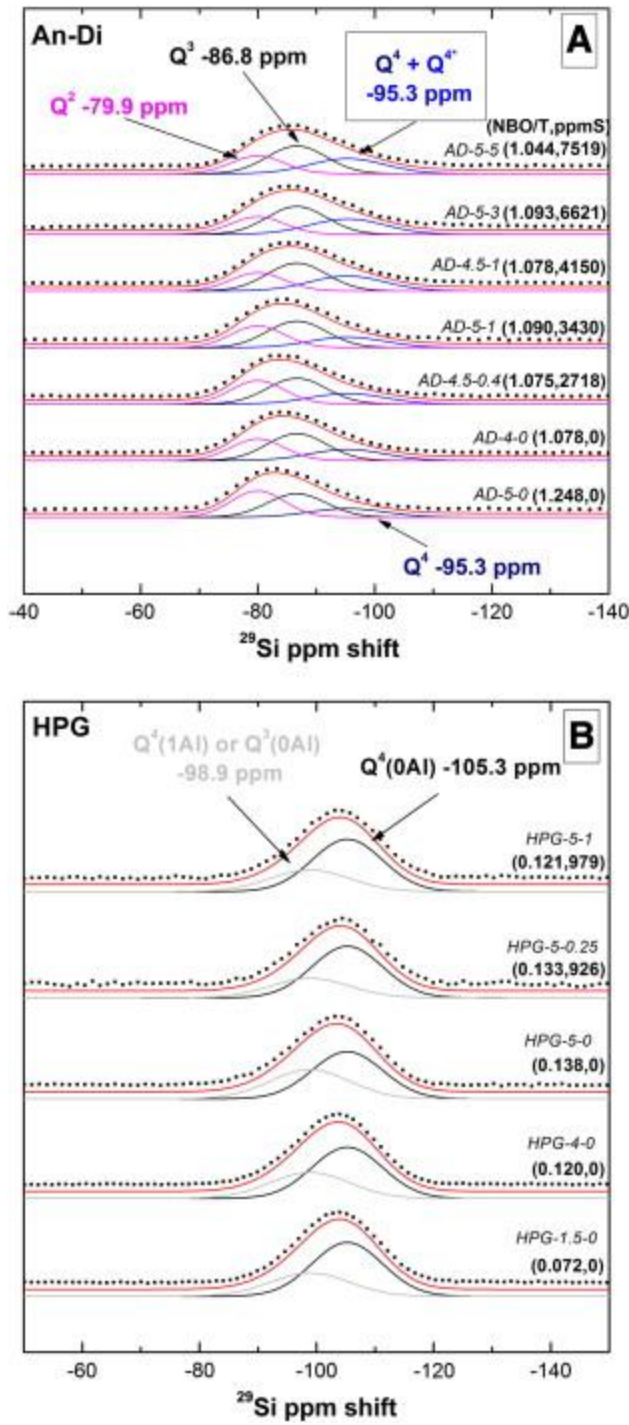


Figure 8: Evolution of the ^{29}Si % species (Q^2 , Q^3 and Q^4 or Q^{4*}) determined by ^{29}Si NMR simulations for An-Di glass samples. A) % Q^n species versus S content. There is a clear trend showing an increase of the Q^4 or Q^{4*} and a decrease of the Q^2 species abundances

as a function of S content consistent with the polymerizing effect of S on the silicate melt structure. B) % Q^n species versus calculated NBO/T. At a constant NBO/T, the S-bearing glasses exhibit a higher polymerization than S-free glass samples. The dashed line indicates the NBO/T value determined for each sample and the total S content is also indicated.

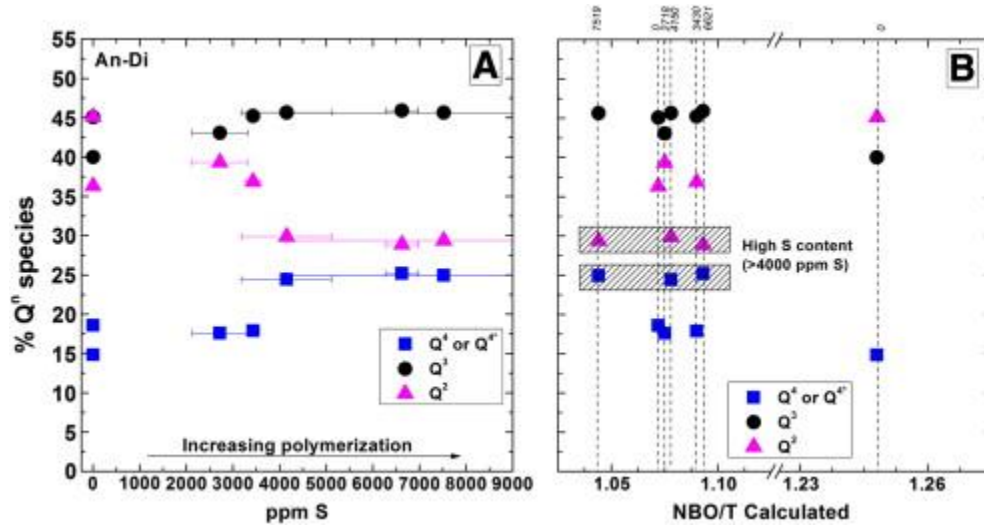


Figure 9: Evolution of the ^{29}Si % Q^n species ($Q^4(0\text{Al})$, $Q^4(1\text{Al})$ or $Q^3(0\text{Al})$) determined by ^{29}Si NMR simulations as a function of the ppm S (A) and Calculated NBO/T (B) for HPG glass samples. The abundance of each Q-species is almost constant as a function of ppm S.

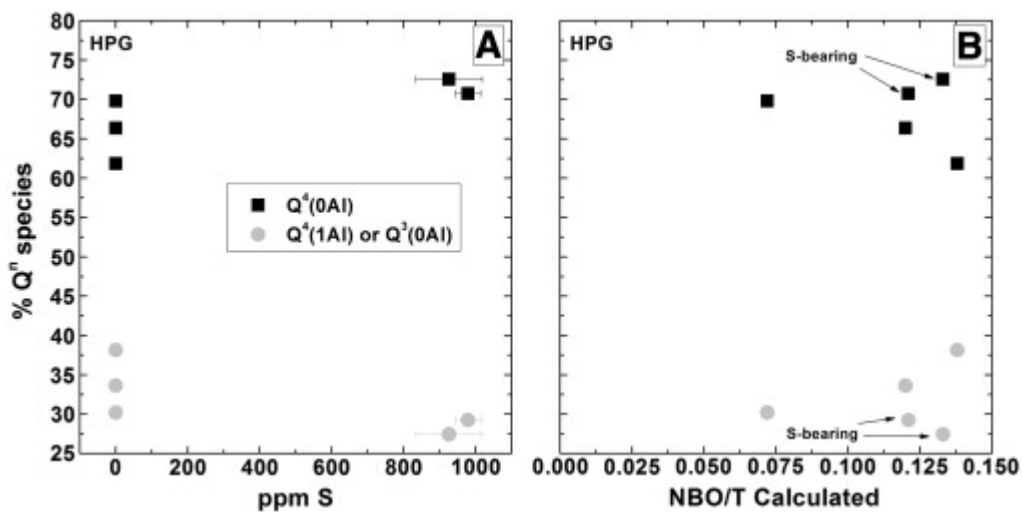


Figure 10: Comparison between Calculated NBO/T in An-Di glass samples calculated from the major element EPMA analyses and the OH concentration and Measured NBO/Si from the ^{29}Si NMR simulations and according to Eq. 5. The Measured NBO/Si is higher than the Calculated NBO/T. S-rich samples show systematically lower measured NBO/Si than the S-poor ones consistent with the polymerizing effect of S on the silicate glass structure.

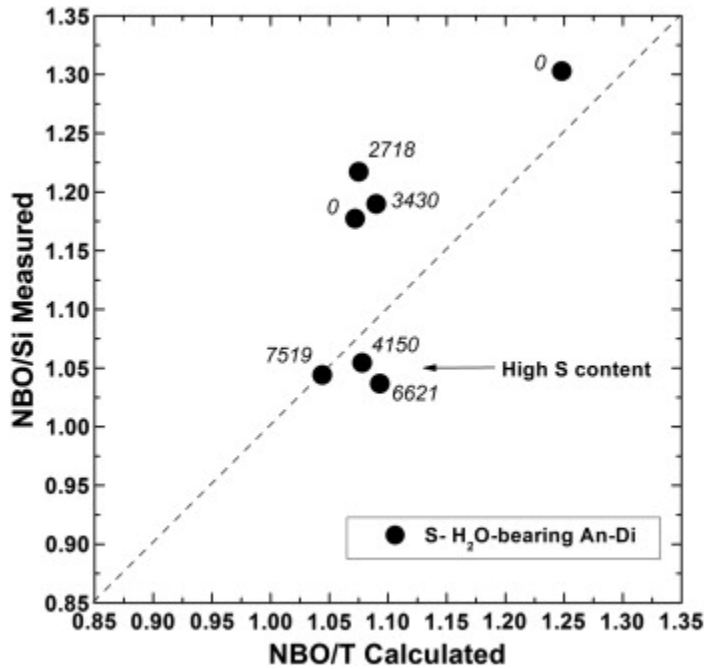


Table caption:

Table 1: Experimental conditions, major elements concentrations in wt.% oxides, initial H_2O content and water speciation determined by FTIR analyses (OH and $\text{H}_2\text{O}^{\text{mol}}$). The NBO/T calculated from the major elements and OH concentrations is also reported. The error reported for major elements concentrations were determined from replicated EPMA analyses on at least 20 points.

Table 2: S content in ppm determined by EPMA analyses from several glass chips. The number of EPMA analytical point for each analytical session is also reported. The average S represents the average calculated from the different analytical sessions. The error is the standard deviation from those analytical sessions.

Table 3: ^{29}Si NMR results: peak maximum determined from Figure 5, simulation results (δ_{iso} , FWHM and % species) for ^{29}Si NMR spectra with three Gaussian peaks for An-Di and AD with various MgO content, with two Gaussian peaks for HPG (see Figure 7). The apparent NBO/Si is also calculated for An-Di samples. The error for each simulated parameter (δ_{iso} and FWHM) is less than ± 0.1 and the error on the abundance of each Q^n species is less than $\pm 0.1\%$ as given by the Origin[®] fitting software package.

Sample s	Press ure (bars)	Major element EPMA analyses (wt.% oxides)						Initi al H ₂ O (wt. %)	Water content from FTIR analyses (wt.%) ^a			<i>f</i> O ₂ (ΔFM Q) ^b	NB O/T ^c
		SiO ₂	Al ₂ O ₃	CaO	MgO	Na ₂ O	K ₂ O		OH conten t	H ₂ O ^{mo} _1 conten t	H ₂ O ^{tot}		
HPG 1250 °C													
HPG theoreti cal ^a		78.6	12.5	0	0	4.6	4.2						0
HPG-5-0	2976	79.74 ± 0.51	12.94 ± 0.19	0	0	3.08 ± 0.55	3.89 ± 0.11	4.76	2.47 ± 0.25	2.92 ± 0.09	5.39 ± 0.30	+ 2.9	0.138
HPG-5-1	2976	79.37 ± 0.81	12.83 ± 0.28	0	0	3.75 ± 0.60	3.91 ± 0.11	4.73	2.02 ± 0.05	2.26 ± 0.13	4.28 ± 0.10	+ 2.6	0.121
HPG-5-0.25	2976	78.74 ± 0.63	13.00 ± 0.19	0	0	3.99 ± 0.19	3.91 ± 0.12	4.92	2.42 ± 0.21	2.62 ± 0.28	4.92 ± 0.08	+ 2.8	0.156
HPG-1.5-0	3204	78.44 ± 1.85	13.45 ± 0.72	0	0	3.95 ± 0.23	3.98 ± 0.16	1.52	1.40 ± 0.09	0.82 ± 0.07	2.23 ± 0.14	+ 1.7	0.072
HPG-4-0	3204	79.14 ± 1.66	13.03 ± 0.19	0	0	3.67 ± 0.10	3.90 ± 0.09	3.90	2.06 ± 0.10	2.20 ± 0.10	4.26 ± 0.06	+ 2.6	0.120
AD 1250 °C													
AD theoreti cal ^a		50.20	15.70	23.40	10.60	0	0						0.921
AD-5-0	3249	51.33 ± 0.38	15.05 ± 0.17	21.39 ± 0.33	11.64 ± 0.18	0	0	4.85	3.31 ± 0.59	1.87 ± 0.13	5.18 ± 0.48	+ 2.8	1.248
AD-5-1	3249	51.35 ± 0.58	15.39 ± 0.33	21.07 ± 0.33	11.84 ± 0.21	0	0	4.77	1.90 ± 0.16	0.91 ± 0.15	2.81 ± 0.27	+ 1.9	1.090
AD-4.5-0.4	3249	51.30 ± 0.51	15.15 ± 0.16	22.77 ± 0.30	10.71 ± 0.16	0	0	4.56	1.62 ± 0.10	1.46 ± 0.10	3.08 ± 0.12	+ 2.0	1.075
AD-5-5	2933	53.21 ± 0.64	15.47 ± 0.10	22.23 ± 0.28	8.91 ± 0.12	0	0	4.89	2.63 ± 0.20	1.05 ± 0.10	3.68 ± 0.13	+ 2.3	1.044
AD-5-3	2933	52.04 ± 0.31	14.58 ± 0.12	24.12 ± 0.20	9.11 ± 0.13	0	0	4.71	1.98 ± 0.06	0.71 ± 0.10	2.70 ± 0.09	+ 1.8	1.093
AD-4.5-1	2933	52.15 ± 0.33	14.82 ± 0.14	23.53 ± 0.25	9.32 ± 0.11	0	0	4.63	2.02 ± 0.24	1.12 ± 0.14	3.14 ± 0.24	+ 2.1	1.078
AD-4-0	3204	51.13 ± 1.25	16.01 ± 0.26	23.30 ± 0.44	9.09 ± 0.15	0	0	3.93	2.39 ± 0.12	1.28 ± 0.14	3.67 ± 0.17	+ 2.3	1.072
AD various MgO volatile-free, 1 bar, 1400 °C													
AD-2 wt.% MgO	1	52.65 ± 0.34	13.99 ± 0.10	25.98 ± 0.17	7.04 ± 0.07	0	0						0.87
AD	1	52.05 ± 0.19	14.37 ± 0.12	24.33 ± 0.26	9.23 ± 0.09	0	0						0.909
AD + 2 wt.% MgO	1	50.59 ± 0.30	13.77 ± 0.10	24.95 ± 0.24	10.63 ± 0.15	0	0						

Table 2. S content in ppm determined by EPMA analyses from several glass chips. The number of EPMA analytical point for each analytical session is also reported. The average S represents the average calculated from the different analytical sessions. The error is the standard deviation from those analytical sessions.

Samples	S from different glass chips	Number of EPMA points for S analyses	Average S (ppm) ^a
<i>HPG 1250 °C</i>			
HPG-5-0			0
HPG-5-1	954 ± 94	20	979 ± 35
	1004 ± 7	47	
HPG-5-0.25	860 ± 138	18	926 ± 93
	992 ± 49	50	
HPG-1.5-0			0
HPG-4-0			0
<i>AD 1250 °C</i>			
AD-5-0			0
AD-5-1	3526 ± 421	30	3430 ± 136
	3334 ± 280	100	
	3561 ± 346	30	
AD-4.5-0.4	2705 ± 121	100	2718 ± 598
	2400 ± 206	60	
	2206 ± 104	50	
AD-5-5	9921 ± 402	21	7519 ± 3397
	5117 ± 107	60	
AD-5-3	6370 ± 414	26	6621 ± 355
	6872 ± 80	59	
	5139 ± 181	29	
AD-4.5-1	4119 ± 90	60	4150 ± 974
	3191 ± 159	50	
AD-4-0			0

a

The average ppm S is obtained from averaging the S content determined for several glass chips from different locations within the recovered glass material and analysed in different analytical sessions. The error corresponds to the standard deviation obtained from the average S content from the different glass chip results.

Table 3. ^{29}Si NMR results: peak maximum determined from Fig. 5, simulation results (δ_{iso} , FWHM and % species) for ^{29}Si NMR spectra with three Gaussian peaks for An–Di and AD with various MgO contents, with two Gaussian peaks for HPG (see Fig. 7). The apparent NBO/Si is also calculated for An–Di samples. The error for each simulated parameter (δ_{iso} and FWHM) is less than ± 0.1 and the error on the abundance of each Q^n species is less than $\pm 0.1\%$ as given by the Origin© fitting software package.

Samples	Peak maximum	Peak 1:	Peak 2:	Peak 3:	Apparent NBO/Si ^d
<i>HPG 1250 °C</i>					
Possible assignment		$\text{Q}^4(1\text{Al})$ or $\text{Q}^3(0\text{Al})$	$\text{Q}^4(0\text{Al})$		
δ_{iso} (ppm) ^{a and c}		-98.9 ± 0.1	-105.3 ± 0.1		
FWHM (ppm) ^b		6.8 ± 0.1	6.0 ± 0.1		
HPG-5-0	-103.8	38.1 ± 0.1	61.9 ± 0.1		
HPG-5-1	-104.0	29.3	70.7		
HPG-5-1 CP	-97.8^e				
HPG-5-0.25	-104.2	27.4	72.6		
HPG-1.5-0	-104.0	30.2	69.8		
HPG-1.5-0 CP	-97.6^e				
HPG-4-0	-103.6	33.6	66.4		
<i>AD 1250 °C</i>					
Possible assignment		Q^2	Q^3	Q^4 and $\text{Q}^{4\Box}$	
δ_{iso} (ppm) ^a		-79.9 ± 0.1	-86.8 ± 0.1	-95.3 ± 0.1	
FWHM (ppm) ^b		4.6 ± 0.1	4.9 ± 0.1	6.4 ± 0.1	
AD-5-0	-82.9	45.1 ± 0.6	40.0 ± 0.5	14.8 ± 1.1	1.303
AD-5-1	-84.8	36.9	45.2	17.9	1.190
AD-4.5-0.4	-84.3	39.3	43.1	17.6	1.217
AD-5-5	-85.7	29.4	45.7	25.0	1.044
AD-5-3	-85.5	28.9	45.9	25.2	1.037
AD-4.5-1	-85.5	29.9	45.7	24.4	1.055
AD-4-0	-84.1	36.3	45.1	18.6	1.177
<i>AD various MgO volatile-free, 1 bar, 1400 °C</i>					
Possible assignment		Q^2	Q^3	Q^4	
δ_{iso} (ppm) ^a		-78.7 ± 0.1	-84.7 ± 0.1	-92.3 ± 0.1	

Samples	Peak maximum	Peak 1:	Peak 2:	Peak 3:	Apparent NBO/Si ^d
FWHM (ppm) ^b		4.6 ± 0.1	5.8 ± 0.1	7.5 ± 0.1	
AD-2 wt.% MgO	- 84.5	23.5	34.2	39.5	0.812
AD	- 83.7	30.5	33.4	36.9	0.944
AD + 2 wt.% MgO	- 82.9	46.0	32.5	23.7	1.245
a					

δ_{iso} represents the chemical shift value in ppm determined from the simulation.